A Lagrangian-Based Approach for Determining Trajectories Taxonomy and Turbulence Regimes

VOLFANGO RUPOLO

Climate and Environment Department, ENEA, Rome, Italy

(Manuscript received 28 October 2005, in final form 6 July 2006)

ABSTRACT

The use of the ratio between the acceleration and velocity time scales $y = T_a/T_v$ to separate Lagrangian trajectories in homogeneous classes is proposed. In fact, when analyzing subsurface floats data in the Atlantic Ocean and surface drifters data in the world's ocean basins, it is observed that trajectories having different values of y are characterized by different shapes, correlation, and dispersal properties. In particular, trajectories having similar values of the acceleration and velocity time scales clearly show the influence of eddies and are characterized by an oscillating velocity correlation function. It is shown here that this trajectory screening is a useful procedure to rationalize the analysis of real Lagrangian trajectories and to avoid a mixture of different regimes, when averaging quantities. The mean statistical quantities computed averaging on quasi-homogeneous datasets put in evidence the role of the coherent structures in the dispersion properties, both in time and in the main oceanic current systems. These results are discussed in the context of the parameterization of eddy diffusivity in general circulation models.

1. Introduction

Surface drifters and subsurface floats have been widely used in the last few decades to study transport properties in the mesoscale range (e.g., Freeland et al. 1975; Riser and Rossby 1983; Rossby et al. 1983; Colin de Verdière 1983; Krauss and Böning 1987; Figueroa and Olson 1989; Zhang et al. 2001; Bauer et al. 2002; Zhurbas and Oh 2003). The main objective of these works was the characterization of the correlation properties of the particle velocities, the study of their dependence on the eddy kinetic energy and the estimate of the absolute dispersion in the mesoscale range. Many of these studies were based on the analysis of single experiments. However, even when considering data collected at the same time in a given geographical area, the analysis of the correlation properties of the Lagrangian velocity field is complex. In fact, the theoretical framework used in these analyses is Taylor's (1921) theory of stationary and homogeneous turbulence but, even inside relatively small subdomains, different regimes of dispersion may exist, because of the huge variability of Lagrangian behaviors (e.g., the coexistence of looping and nonlooping trajectories; Veneziani et al. 2004). Consequently, the computation of statistical parameters by means of simple and unconditioned means among Lagrangian trajectories experiencing different flow regimes may give rise to misleading results. The complicated nature of Lagrangian dispersion has been evidenced also using simplified conceptual models. For instance, Elhmaidi et al. (1993) and Pasquero et al. (2001), in the context of quasigeostrophic 2D turbulence, have shown that to correctly model dispersal properties, one should consider at least two different regimes. Namely, distinguishing particles trapped in energetic coherent structures from those floating in a more quiescent turbulent background. More recently, Berloff and McWilliams (2003), to represent the huge Lagrangian variability, have used stochastic models in which the decorrelation parameters vary with statistical properties given by a probability distribution obtained from data. In the past there was some effort to avoid a mixture of different regimes computing statistical quantities averaging between Lagrangian trajectories that were previously subdivided in kinematically quasi-homogeneous subdatasets considering as screening indices either the eddy kinetic energy and the Lagrangian correlation time (Rupolo et al.

Corresponding author address: Volfango Rupolo, Climate Department, ENEA, Via Anguillarese 301, 00123 Rome, Italy.
E-mail: rupolo@casaccia.enea.it

DOI: 10.1175/JPO3038.1

1996) or the mean vorticity of the trajectory (Veneziani et al. 2004).

Nowadays, public archives contain a massive quantity of Lagrangian data collected since the late 1970s at different depths and in all World Ocean basins. An integrated analysis of this dataset, even if difficult for the aforementioned problems, would be of fundamental importance for the understanding of the ocean transport properties. Hence, considering important to define an experimental procedure to compute Lagrangian statistical properties through averages on quasi-homogeneous subdataset, we propose here a data processing technique to separate the whole dataset in classes of trajectories morphologically homogeneous and characterized by different regimes of dispersion and by different qualitative behavior of the velocity correlation function. The statistical properties computed averaging on such subdatasets are then used, first, to investigate kinematics relations in the different regimes and, second, to map in the geographical space the quantitative relevance of these different regimes.

The screening of the trajectories is done using the ratio between the acceleration and velocity time scales $y = T_a/T_v$. The motivation for the choice of the index $y = T_a/T_v$ is simple and is based upon the following considerations. Any real particle, because of its inertia, cannot be subjected to infinite acceleration and consequently the correlation time scale of the Lagrangian acceleration has to be different from zero, perhaps in a time range smaller than the observational time sampling. On the other hand, many previous studies (e.g., Zambianchi and Griffa 1994; Griffa 1996) have shown that, especially the motion of surface drifters but in some case also of subsurface floats, may be well represented by first-order stochastic model, in which $T_v \neq 0$ but $T_a = 0$. In this case, the motions that in the time sampling scale appear to be dynamically uncorrelated are highly energetic; the corresponding Lagrangian trajectory is often characterized by a well-defined slow frequency motion perturbed by jumps in the position and discontinuities in the velocity field. In contrast, if also $T_a \neq 0$ a relevant part of the energy of the motion of the Lagrangian device is absorbed by dynamically correlated movements, the trajectory is smoother and the corresponding velocity field does not show discontinuities.

Hence, considering all the available world's ocean surface drifters and the Atlantic Ocean subsurface floats data of the World Ocean Experiment (WOCE) archive, we will compute for each trajectory the ratio $y = T_a/T_v$ and we will separate the trajectories in different classes characterized by different values of y, showing the greater homogeneity of trajectories belonging to the same class in terms of shape, velocity correlation properties, and of relationships between eddy kinetic energy and correlation length scale. Then, we will show that the simple computation of the relative importance of the different classes of trajectories in the different geographical areas allows for a characterization of the dispersal properties of the main oceanic currents. This analysis is useful to detect how and where the presence of coherent structures influences the Lagrangian dispersion, something that may advance the representation of the eddy diffusivity in the ocean general circulation models (OGCMs).

The estimate of the velocity and acceleration correlation time scales will be done using, as a paradigm of the observed ocean variability, a second-order Lagrangian Stochastic Model (LSM), since this simple model directly allows for a simple estimation of the characteristic time scales from individual trajectories. All of the analysis of the present work will be done assuming that also the subsurface float moves on a two-dimensional surface.

The work is organized as follows. In section 2 we define the statistical functions to be used and derive some simple algebraic relations from the second-order LSM. In section 3 we select the different classes of trajectories by means of the dimensionless index $y = T_a/T_v$, showing that they can be considered as representative of different regimes of dispersion. In section 4, studying the geographical distribution of the relative weight of each class, we will characterize the main oceanic currents identifying where the role of the coherent structures is important. In section 5 we give a summary and further discuss the results in the context of eddy diffusivity parameterization in OGCMs.

2. Functions definition and second-order LSM

In this section, we shall introduce the statistical functions that are commonly used when analyzing Lagrangian data and we shall derive some simple algebraic relations from the second-order LSM, considering, for simplicity, the 1D space. The generalization to the 2D case is straightforward assuming the homogeneity of the velocity field.

Given a velocity time series $u(t)$, the velocity correlation function (1), its power spectrum (2), and the single-particle dispersion (3) are descriptions that are mathematically equivalent but complementary:

$$R(\tau) = \lim_{T \to \infty} \frac{1}{\sigma_U^2 T} \int_0^T u'(t + \tau)u'(t)\, dt, \qquad (1)$$

$$P(\nu) = \int_0^\infty R(\tau)\cos(\pi\nu\tau)\, d\tau, \quad \text{and} \qquad (2)$$

$$A(t) = \langle |x'(\tau + t) - x'(\tau)|^2 \rangle. \quad (3)$$

Here $x(t)$ is the position, $u'(t) = u(t) - U$, where $U = (N - 1)^{-1}\Sigma_{j=1}^{N-1} u(j)$ is the time-averaged velocity, $x'(t) = x(t) - Ut$, σ_U^2 is the eddy kinetic energy, and the angle brackets indicate an average over the time lag t.

The Lagrangian integral time T_L is a measure of the time correlation of the velocity time series and is defined as

$$T_L = \int_0^\infty R(\tau)\, d\tau. \quad (4)$$

The single-particle dispersion (3) is related to the velocity correlation function $R(t)$ and to the power spectrum $P(\nu)$ by the relations

$$A(t) = 2\sigma_U^2 \int_0^t (t - \tau) R(\tau)\, d\tau \quad \text{and} \quad (5)$$

$$A(t) = \frac{1}{\pi^2} \int_0^\infty \frac{P(\nu)}{\nu^2} \sin^2(\pi\nu t)\, d\nu. \quad (6)$$

Taylor's (1921) result in form (5) and (6) is due to Kampé de Fériet (1939).

For small times, $\sin^2(\pi\nu t) \sim (\pi\nu t)^2$ and (6) becomes (ballistic regime)

$$A(t) \sim t^2 \int_0^\infty P(\nu)\, d\nu = \sigma_U^2 t^2 \quad \text{for} \quad t \ll T_L, \quad (7)$$

and, for large times, it can be shown (e.g., Krauss and Böning 1987) that the other asymptotic behavior holds:

$$A(t) = P(0)t = 2\sigma_U^2 T_L t \quad \text{for} \quad t \gg T_L. \quad (8)$$

For small times (7), all frequencies equally contribute to particle displacements, whereas, for large times (8), the lower frequencies dominate and, if the velocity spectrum saturates at small frequencies, the Lagrangian diffusivity $K(t) = (1/2)(d/dt)A(t)$ asymptotically approaches the constant value (random walk or Brownian regime):

$$K(t) = \sigma_U^2 T_L, \quad \text{for} \quad t \gg T_L. \quad (9)$$

In a real trajectory, the variances of the velocity and acceleration time series are finite and consequently the following constraints on the spectral shape hold:

$$\int_0^\infty P(\nu)\, d\nu = \sigma_U^2 < \infty \quad \text{and}$$
$$\int_0^\infty \nu^2 P(\nu)\, d\nu = \sigma_A^2 < \infty. \quad (10)$$

This means that the high-frequency spectral decay is bounded by a logarithmic spectral slope α that satisfies

$$\alpha > 3 \quad \text{for} \quad \text{large } \nu. \quad (11)$$

This high-frequencies asymptotic behavior, which may occur in a frequency range not resolved by the time sampling interval, is due to the inertia of the Lagrangian particle that cannot be subjected to infinite accelerations. Condition (11) is equivalent to a constraint for the velocity correlation function that in this case is characterized by a smooth quadratic behavior for small times.

Experimental spectra from Lagrangian floats (Colin de Verdière 1983; Krauss and Böning 1987; Rupolo et al. 1996; Lumpkin and Flament 2000) and from long time series of altimetric Ocean Topography Experiment (TOPEX)/Poseidon data in the extratropical ocean (Stammer 1997) are characterized by a low-frequency (wavenumber) plateau and by a decay in the mesoscale range with bilogarithmic spectral slope $2 < \alpha < 3$. In regions characterized by strong mesoscale activity the asymptotic behavior (11) are often observed and the velocity correlation function may also show oscillations, due to the spiraling of fluid particles trapped in coherent structures.

Second-order LSM

In this model the random discontinuity is introduced in the acceleration a and the incremental equations are

$$\frac{dx}{dt} = U + u, \quad (12)$$

$$\frac{du}{dt} = a - \frac{u}{T_\nu}, \quad \text{and} \quad (13)$$

$$\frac{da}{dt} = -\frac{a}{T_a} + \frac{[2\sigma_U^2(T_a + T_\nu)]^{1/2}}{T_\nu T_a} \frac{dw}{dt}, \quad (14)$$

in which, using the previous definitions, the stochastic impulse is represented by a random increment $dw(t)$ from a normal distribution with zero mean and variance dt. Equations (12)–(14) are equivalent to the second-order stochastic process

$$\frac{d^2u}{dt^2} + \alpha_1 \frac{du}{dt} + \alpha_2 u = (2\sigma_U^2 \alpha_1 \alpha_2)^{1/2} \frac{dw}{dt}, \quad (15)$$

with $\alpha_1 = (1/T_\nu) + (1/T_a)$ and $\alpha_2 = 1/(T_a T_\nu)$.

This model has been introduced by Sawford (1991) to correct the small-scale behavior of the first-order LSM in the description of flows at high, but finite, Reynolds number. The two characteristics time scales T_a and T_ν respectively represent the correlation of the forcing and the memory of the velocity induced by, high-frequency, uncorrelated impulses (Griffa 1996).

The correlation function of the velocity field obtained integrating (12)–(14) is given by

$$R(t) = \frac{\beta_2 e^{\beta_1|t|} - \beta_1 e^{\beta_2|t|}}{\beta_2 - \beta_1}, \tag{16}$$

where

$$\beta_{1,2} = \frac{-\alpha_1 \pm \sqrt{\alpha_1^2 - 4\alpha_2}}{2} \tag{17}$$

are roots of $z^2 + \alpha_1 z + \alpha_2 = 0$ and are equal to $\beta_1 = -(1/T_v)$ and $\beta_2 = -(1/T_a)$ (Sawford 1991). It is easy to show (Berloff and McWilliams 2002) that the following relation holds:

$$\frac{1}{T_v T_a} = \frac{\sigma_A^2}{\sigma_U^2}, \tag{18}$$

where σ_U^2 and σ_A^2 are the velocity and acceleration variances. The Lagrangian correlation time T_L, obtained integrating (16), is equal to

$$T_L = T_v\left(1 + \frac{T_a}{T_v}\right), \tag{19}$$

which means that when $T_a \neq 0$ the finite acceleration contributes to increase the correlation of the velocity field.

Depending on the sign of the radicand in (17), we have that

$$T_v, T_a \in R \quad \text{for} \quad \alpha_1^2 \geq 4\alpha_2$$

and

$$T_v, T_a = a \pm ib \in C \quad \text{for} \quad \alpha_1^2 < 4\alpha_2.$$

The appearance of a complex conjugates pair of time scales is symptomatic of a missing but dynamically important spatial dimension. Reynolds (2002) has examined the correspondence between multidimensional $(n-1)$th-order LSM and one-dimensional nth-order LSM. In the parameter range in which $T_v, T_a \in C$, the 1D second-order LSM is then equivalent to a 2D first LSM with spin, where the nonisotropy of the velocity field is expressed by a preferred sense of rotation about the vertical axis to simulate spiraling particles motion (Borgas et al. 1997).

For $t \sim 0$, $R(t)$ defined by (16) is characterized by a smooth behavior, as is expected in flow with finite acceleration, while for $t \gg T_a$ the correlation function asymptotes to the exponential form characteristics of the first-order LSM. In this model, when $T_a > 0$, the variance of both velocity and acceleration is finite, and for $T_a \to 0$ relation (15) becomes a first-order equation and the model collapses to a first-order LSM.

3. Dataset and trajectories taxonomy

a. Subsurface floats dataset

Since we are interested in computing eddy kinetic energy and velocity decorrelation time scales in this work we have to consider only continuously (acoustically) tracked SOFAR and RAFOS floats. In particular we analyze subsurface floats downloaded from the WOCE (2002) archive moving at a nominal depth between 400 and 1000 m in the Atlantic Ocean, since only there does the data density allows for a reliable statistics. In the WOCE dataset, the data are divided per experiment and in Table 1 we list the experiments considered in this work. The floats are neutrally buoyant, ballasted for a specific pressure or density surface. Most of the floats considered here were isobaric, but those in the North Atlantic Current, Western Boundary Current, Atlantic Climate Change Experiment (ACCE), Canary Islands Azores Gibraltar Observations (CANIGO), and Cape of Good Hope Experiment (KAPEX) were quasi-isopycnal and thereby occupying a range of depth. Recent analyses including both isobaric and isopycnal floats (Lacasce 2000; Lacasce and Bower 2000) showed no systematic differences between the two datasets, even considering relative dispersion, that may be amplified by the vertical shear. So, in the following, because of the lack of continuously tracked subsurface trajectories, we will consider data from both isopycnal and isobaric instruments.

The depth interval (400–1000 m) was chosen since we are interested in studying the geostrophic turbulence that at this depth is intensified by the energetic transfer from the high to the first baroclinic mode (Shafer Smith and Vallis 2001). At greater depth, below the permanent thermocline, the turbulent activity is smaller and the float motion is dominated by low-frequency wave and by topographic constraint.

Subsurface floats data positions were mostly recorded every 24 h and when a different time step was used, positions and velocity were interpolated to have a daily time sampling. Gaps in the original time series smaller than four consecutive points were linearly interpolated. When larger gaps were found, the original trajectory was divided in more pieces.

To fully resolve the mesoscale frequency range and to minimize the effects of the nonhomogeneity of the velocity field, we perform correlation analysis on pieces of trajectories of uniform length of 64 days. For the Atlantic Floats (AF) dataset, our analysis is the based on 2074 pieces of 64-day-long trajectories, for a total of 132 736 daily observations (see Table 3).

TABLE 1. List of SOFAR and RAFOS experiments. For each experiment are given the principal investigator, institution, geographical area, and number of 64-day-long trajectories considered here; S is SOFAR and R is RAFOS.

Experiment	Principal investigator	Institution(s)	Area	No.	First year	Float type
Pre–Local Dynamics Experiment (LDE)	Rossby	University of Rhode Island (URI)	Northwest North Atlantic	93	1975	S
LDE	Rossby	URI	Northwest North Atlantic	32	1978	S
Gulf Stream	Richardson, Price, Schmitz Owens, Rossby	Woods Hole Oceanic Institution (WHOI), URI	Northwest North Atlantic	5	1979	S
Gulf Stream recirculation	Richardson, Price, Schmitz, Owens, Rossby	WHOI, URI	Northwest North Atlantic	87	1980	S
Site L	Owens, Price	WHOI	Northwest North Atlantic	107	1982	S
Topographic Gulf Stream Experiment (TOPOGULF)	Ollitraut	French Research Institute for the Exploitation of the Sea (IFREMER)		168	1983	S
Eastern Basin	Price, Richardson	WHOI	Eastern North Atlantic	13	1984	S
Newfoundland Basin	Owens	WHOI	Northwest North Atlantic	34	1986	S
Iberian Basin	Zenk, Boebel	Institut für Meereskunde (IFM)	Eastern North Atlantic	27	1990	R
Brazil Basin	Boebel, Zenk	IFM	Western South Atlantic	275	1992	R
North Atlantic Meddies	Richardson	WHOI	Eastern North Atlantic	22	1993	R
North Atlantic Current	Rossby, Prater	URI	Northwest North Atlantic	147	1993	R
Meddy Seeding	Bower	WHOI	Eastern North Atlantic	15	1993	R
Western Boundary Current	Bower	WHOI	Northwest North Atlantic	70	1994	R
EUROfloat	Gould, Zenk, Williams, Speer, Cantos	Various	Eastern North Atlantic	59	1995	R
ACCE	Bower	WHOI	Northeast North Atlantic	523	1996	R
ACCE	Rossby, Prater, Carr	URI	Northeast North Atlantic	134	1997	R
CANIGO	Ambra, Kantos, Knoll	Various	Eastern North Atlantic	33	1997	R
KAPEX	Boebel, Rossby	University of Cape Town (UCT), URI	Southeast South Atlantic	188	1997	R

b. Surface drifters dataset

In this work we analyze surface drifters data collected from 1979 to October 2005 in the context of the Global Drifter Program (GDP; online at http://www.aoml.noaa.gov/phod/dac/gdp.html), formerly WOCE Surface Velocity Program (WOCE/SVP). The Marine Environmental Data Services (MEDS; http://www.meds-sdmm.dfo-mpo.gc.ca) archives and posts all data collected and processed by the Atlantic Oceanographic and Meteorological Laboratory (AOML; http://www.aoml.noaa.gov) under the GDP. We downloaded data from 1979 to 2003 from the WOCE (2002) and MEDS archives in which the Lagrangian data are grouped for year and divided geographically in four subdatasets for the Atlantic, Arctic, Pacific, and Indian Oceans (see Fig. 1). Data from 2004 to 2005 were downloaded directly from the AOML archive.

Drifters are tracked by the Argos satellites with an estimate of accuracy of position of about 150–1000 m. The AOML's Drifter Data Assembly Center (DAC) perform a first quality control of the data (see, e.g., Lumpkin and Pazos 2007) and then interpolates the raw fixes to uniform 6-h interval using an optimal procedure known as kriging (Hansen and Poulain 1996). Besides the interpolated positions the DAC provides also an estimate of the error on the position, which becomes very useful in identifying accidental or programmed gaps on the data transmission. Measuring surface currents with Lagrangian instruments was an important challenge for centuries and instruments and techniques continuously evolved with time until the modern satellite-tracked surface drifters. History of the Lagrangian surface devices and the description of the evolution of different techniques can be found in Lumpkin and Pazos (2007). Here it is interesting to note that from the eighties, and under the request of the World Climate Research Program, efforts were made to deploy standardized surface drifters. In particular, the modern set of SVP data is made with drifters drogued at a depth of 15 m. The data downloaded from MEDS (2001–03) and AOML (2004 and 2005) are all collected using drifter drogued at this depth. Nevertheless, in the WOCE (2002) archive from 1979 to 2000 are included also few drifters drogued at different depth. The first screening of the downloaded dataset then consists in retaining

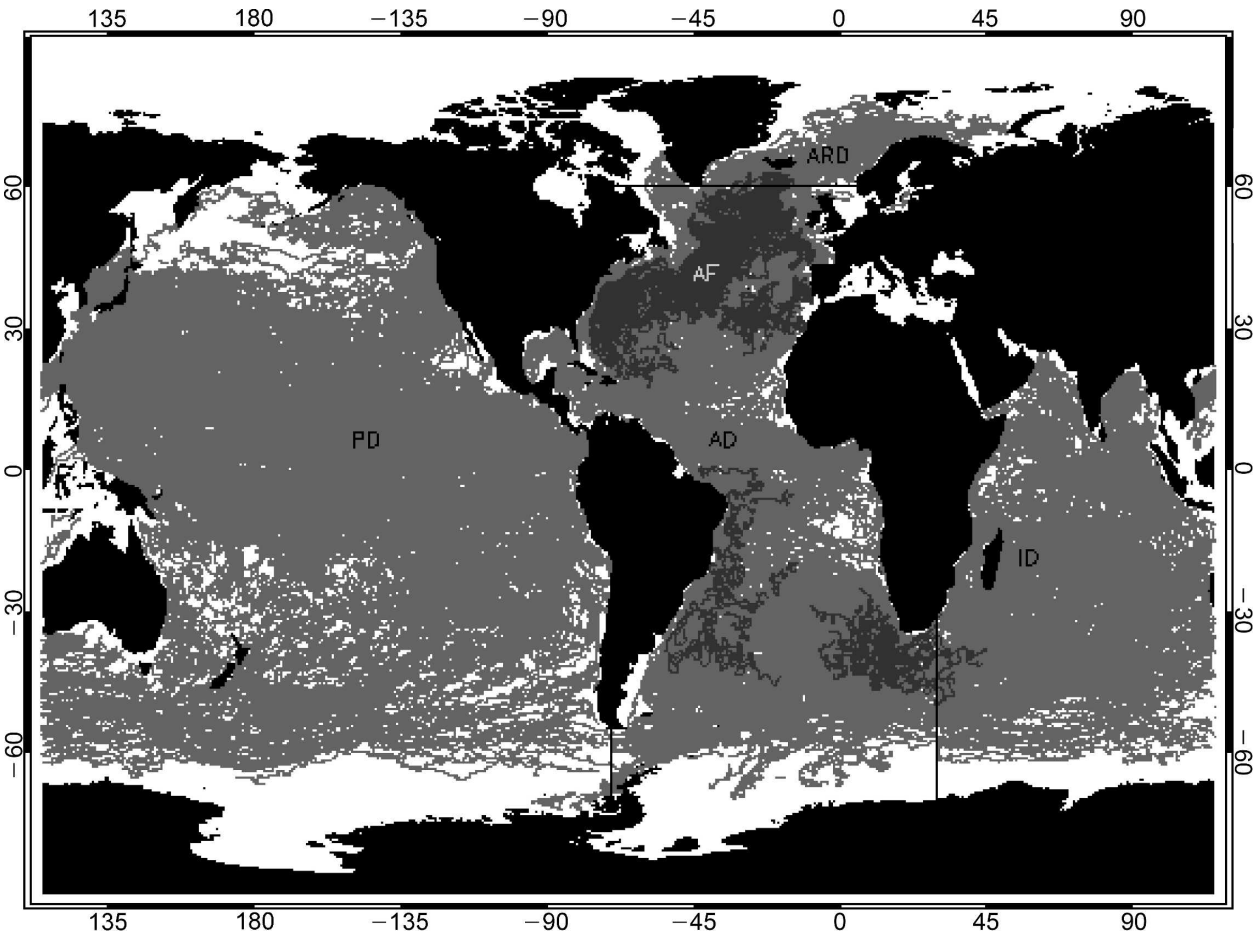

FIG. 1. The Lagrangian datasets used in this work. Black and gray lines refer to subsurface floats and surface drifters. The AD dataset is delimited by 60°N, 70°E, and 30°W. Arctic drifters are all in the Atlantic Sea north of 60°N. The ID and PD datasets are divided at 115°W (trajectories northeast of Indonesia belong to the PD dataset).

only drifters with the drogue between 0 and 50 m. Doing that we reject 403 drifters (over a total of 8091 from 1979 to 2000) for which the drogue depth is not specified or it is greater than 50 m. The 92% of the retained drifters have a drogue depth between 15 and 15.4 m and only about the 2.8% (1.4%) are drogued at a depth smaller than 10 m (greater than 20 m).

Coherently with the AF dataset, also for the surface drifters we consider pieces of trajectories of uniform length of 64 days. This relatively large dataset of pieces of 64 days long of trajectories is subsequently screened in order to eliminate segments affected by accidental or programmed gaps in the transmission of data. In fact, to save battery power, older drifters often used a duty cycle of ⅓, typically with the transmitter spent one day on then two days off. Many drifters were also programmed to transmit continuously for a first period to subsequently switch to an alternating mode of transmission. Moreover, the DAC interpolates positions, when occasional gaps in the transmission days are present. Since we are interested in computing decorrelation time scales, the presence of such drifters could lead to significant biasing in our results. Unfortunately, the metadataset does not contain exhaustive information about transmission gaps for all the drifters. Consequently, we adopt the technique of individuate drifters (or pieces of trajectory of drifters) transmitting not continuously looking at the power spectrum of the errors on the position. As an example, drifters working with a 1-day on 2-days off ⅓ duty cycle, display a well-defined peak at the frequency ⅓ days^{-1}. In particular, inspecting trajectories for which information on the duty cycle is given (using a routine kindly furnished by R. Lumpkin) we select threshold values useful to automatically detect on the spectrum of the error the peaks induced by the transmission gaps. Accidental and isolated gaps in the transmission are identified imposing threshold values both on the magnitude of the error and in the

low frequency content of the error spectra. The entire dataset (42 813 pieces of 64-day-long trajectories, for the four basin) is then screened in order to eliminate peaks and to obtain an approximately white spectrum of the position error, for frequency range smaller than 1 day^{-1}. With the chosen threshold values about the 40% of 64-day-long trajectories are rejected.

All of the surface drifters data were recorded every 6 h; in our analysis we retain this time step but, to filter out energy in the frequency range $\nu >$ day^{-1}, a further smoothing of the positions time series $y_i(j)$ is performed through a boxcar average of width 2,

$$x_i(j) = \frac{1}{5}\sum_{l=-2}^{2} y_i(j + l),$$

before computing the velocities from the smoothed time series $x_i(j)$ by

$$u_i(j) = \frac{1}{\Delta t}[x_i(j + 1) - x_i(j)],$$

where $\Delta t = 6$ h and the index $i = 1, 2$ refers to the zonal and meridional directions. This further smoothing was performed in order to avoid the influence of inertial and subinertial motions on the experimental estimate of the correlation time scale and its effect on the results of this work will be discussed in the following.

Last, to reject trajectories affected by anomalous noise in the high-frequency range, we reject all the (surface and subsurface) trajectories (<1%) with $T_L < 0.75$ days (see below for the experimental definition of the Lagrangian correlation time T_L). We end up with 2074, 7333, 561, 12 154, and 2969 pieces of 64-day-long trajectories for the Atlantic Floats (AF), Atlantic Drifters (AD), Arctic Drifters (ARD), Pacific Drifters (PD), and Indian Drifters (ID) datasets, for a total of 132 736 and 1 473 088 daily observations for the subsurface floats and surface drifters datasets, respectively. Details of the datasets are given in Tables 1–3, and in Figs. 1 and 2 we show all Lagrangian trajectories (black lines for the subsurface ones) considered in this work and a map of daily observations per 1° square bin.

In Fig. 3 we show the mean zonal and meridional spectra and in Fig. 4 we plot the mean total velocity correlation functions (semisum of the correlation functions of the zonal and meridional velocities) for the five datasets. Although these quantities are obtained by averaging on a mixture of dynamics distributed geographically, some considerations can be made:

1) The subsurface floats are less energetic than the surface drifters (see also Table 4) and the latter ones, especially in the Pacific, display a well-defined anisotropy in the low-frequency energy content (Fig. 3), showing that the zonal variability is inherently more energetic at lower frequencies (Krauss and Böning 1987).
2) The Lagrangian meridional velocity spectra are similar to the generic shape evidenced by Stammer (1997) analyzing TOPEX/Poseidon altimetric data and are characterized by a low-frequency plateau followed by a spectral decays. Since the Lagrangian time scales are typically smaller than the Eulerian ones (e.g., Middleton 1985), in the Lagrangian spectra the break between the plateau and the spectral decays is observed at frequencies [$\sim$(20 days)$^{-1}$] higher than in the Eulerian ones [$\sim$(250 days)$^{-1}$];

TABLE 2. Number of original trajectories of drifters drogued at depth z: $0 < z < 50$ m for each year.

	AD	ARD	PD	ID
1979	—	—	40	—
1980	—	—	72	—
1981	—	—	23	—
1982	—	—	32	—
1983	—	—	35	—
1984	—	—	29	—
1985	—	—	31	2
1986	—	—	71	8
1987	—	—	153	1
1988	—	1	285	—
1989	20	—	323	—
1990	54	—	363	10
1991	62	23	426	9
1992	115	73	575	14
1993	198	86	629	11
1994	208	42	588	23
1995	260	43	620	162
1996	317	66	728	191
1997	358	84	504	190
1998	381	34	464	126
1999	466	42	625	166
2000	410	20	594	179
2001	433	9	589	191
2002	454	16	541	205
2003	509	18	682	201
2004	582	16	895	208
2005	659	18	1036	215

TABLE 3. Number of 64-day-long trajectories considered in this work and daily observations for the five datasets and for all the surface drifters data.

	No. of trajectories	No. of days
AF	2074	132 736
AD	7333	469 312
ARD	561	35 904
PD	12 154	777 856
ID	2969	190 016
All drifters	23 017	1 473 088

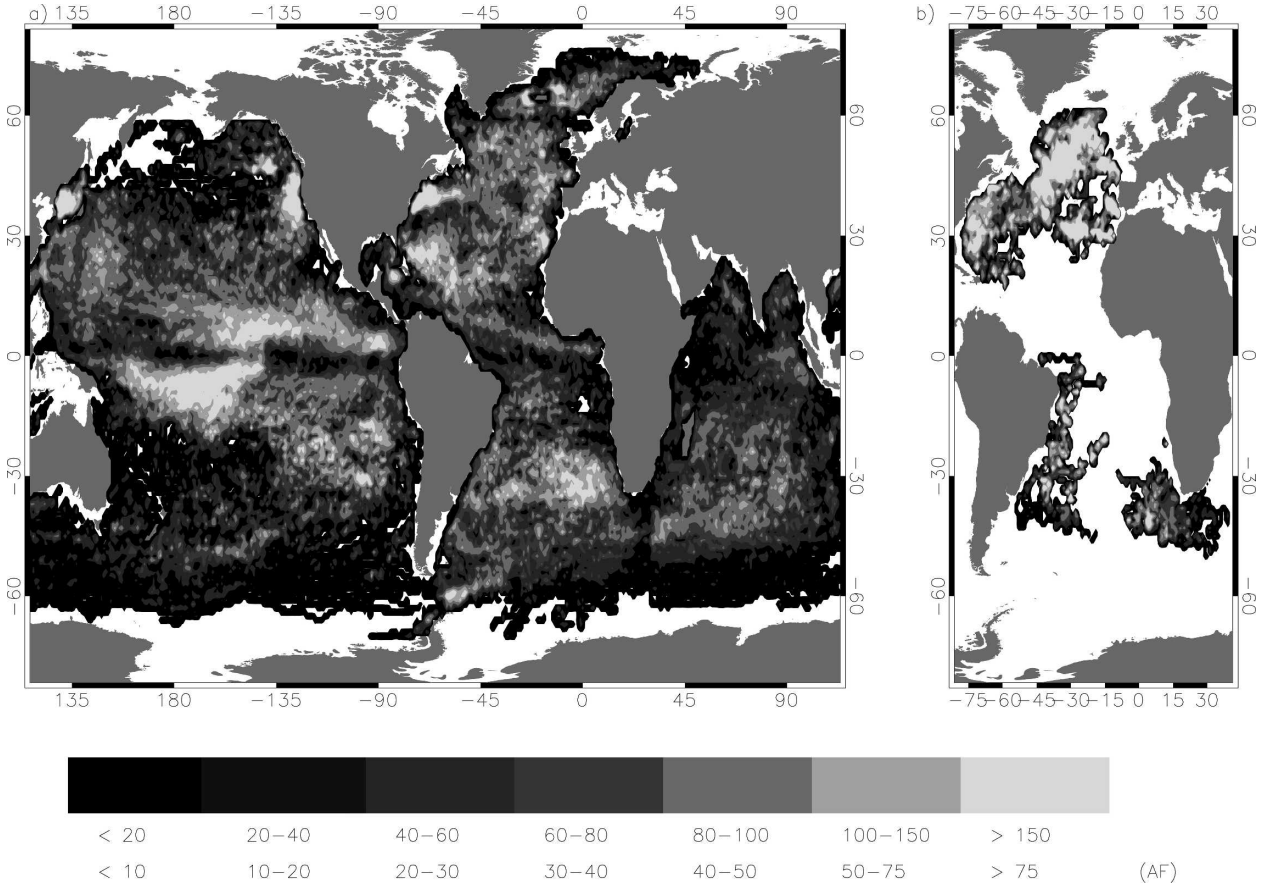

FIG. 2. Map of number of daily observations per 1° square bin for (a) the surface drifters and (b) subsurface floats. The upper (lower) numbers in the shade scale refer to the surface drifters (subsurface floats) dataset.

3) even if subsurface floats data were mostly recorded in areas where the motion is characterized by a massive presence of coherent structures, like the Gulf Stream and Agulhas currents or the Mediterranean outflow area, no striking qualitative differences (except for the anisotropy) are observed between the spectra and velocity correlation functions of the float and drifters datasets, nor in the spectral slope decay or in the shape of the velocity correlation function (oscillations and small times behaviors). In particular, all the mean velocity correlation functions have an exponential like behavior for $t \to 0$.

c. *Trajectories taxonomy*

Here, we will not discuss the anisotropy of the spectral and transport properties but we will use the index $y = Ta/Tv$, computed for each trajectory, to individuate subdatasets of trajectories morphologically similar and characterized by having more homogeneous correlation and dispersion properties.

The estimate of the Lagrangian correlation time T_L is obtained from Eq. (4) integrating in the first positive lobe the zonal and meridional components of the experimental velocity correlation (1) and then considering T_L as the semi sum of the two values. This first zero crossing technique, even if ill founded, is commonly used [for a discussion of the different techniques used in the literature see Lumpkin et al. (2002)]. In particular, the use of the first zero crossing technique may lead to overestimate time scales, especially in presence of spiraling trajectories characterized by having velocity autocorrelation function with deep negative lobes. On the other hand, dropping the mean velocity of the time series will tend to underestimate the time scale, since low-frequency variability is eliminated. Last, when computing Lagrangian time scales with trajectory data one has to consider that, whatever the technique, the final estimate is also depending on the size of the time sampling. Obviously a better estimate is obtained with a smaller size of the time sampling. It can be shown subsampling original trajectories with small sampling time (e.g., Storch and Zwiers 1999), that a reliable es-

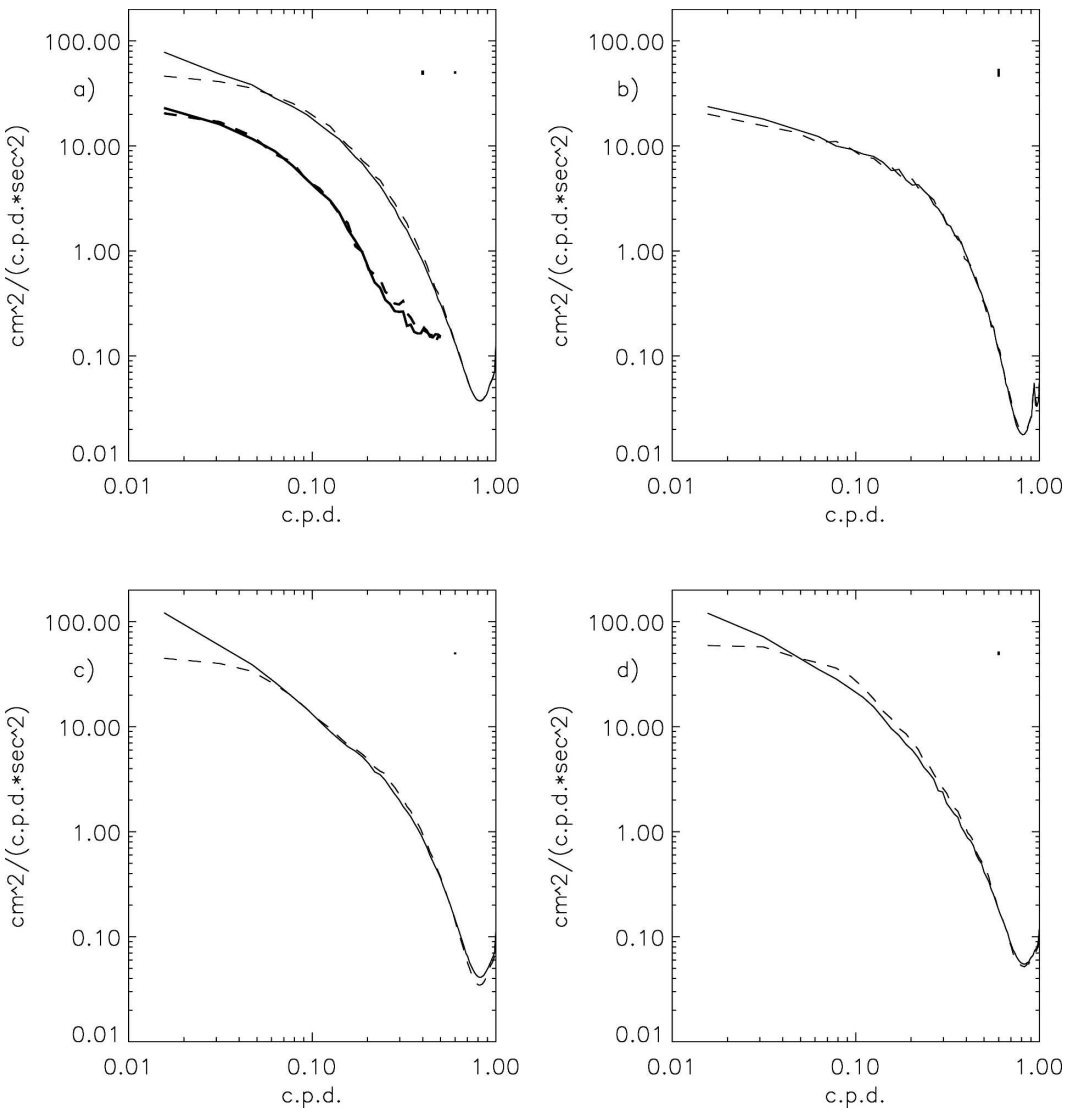

FIG. 3. Zonal (continuous line) and meridional (dashed line) velocity spectra for the five datasets. (a) The thick and thin lines refer to the AF and AD datasets. Spectra for the (b) ARD, (c) PD, and (d) ID datasets. The 95% confidence level is indicated by the vertical bar in the top right part of the panel and it is computed assuming that the power spectra follow a $\chi^2(2N)$ distribution, where N is the number of the trajectories for each dataset.

timate is obtained with a ratio $\Delta t/T_L \leq 0.2$–0.25. When this ratio is greater, the computation of T_L will give raise to an overestimate. Looking at the values of T_L in Table 4 and considering that the time sampling is 24 and 6 h for the floats and drifters data we can see that in some cases we are near the threshold limit. In general, when calculating Lagrangian time scales some approximations are inevitable and the specific value of the decorrelation time may be not very informative. However, comparison between time series with the same time sampling and uniformly computed indicates which processes have large memory.

With this limitation in mind, we proceed and for each trajectory we obtain the estimate of T_v and T_a using relations (18) and (19), which give

$$T_v = \frac{T_L + \sqrt{T_L^2 - 4\dfrac{\sigma_U^2}{\sigma_A^2}}}{2} \quad \text{and}$$

$$T_a = \frac{T_L - \sqrt{T_L^2 - 4\dfrac{\sigma_U^2}{\sigma_A^2}}}{2}, \tag{20}$$

where, for each trajectory, the Lagrangian eddy kinetic energy $\sigma_U^2 = (1/2)(\sigma_{u_1}^2 + \sigma_{u_2}^2)$ and the acceleration vari-

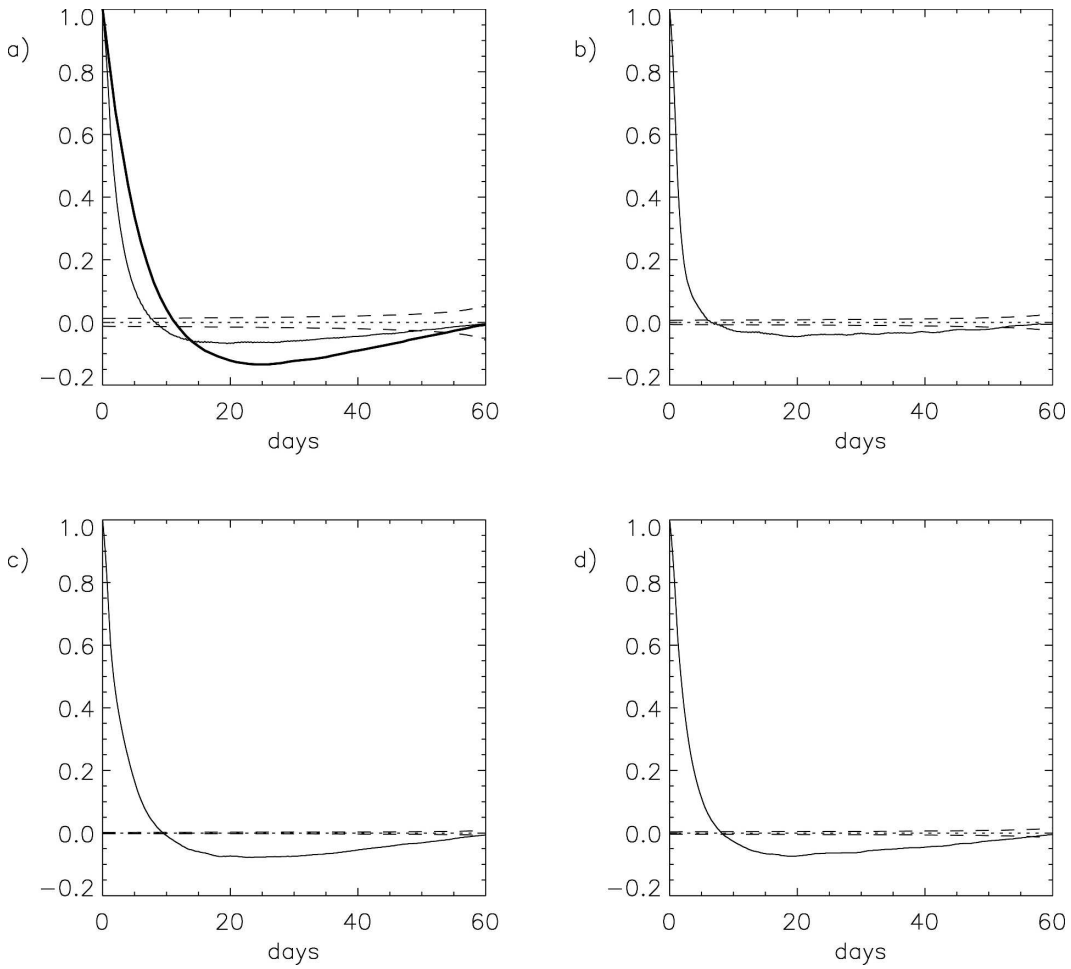

FIG. 4. (a) Total velocity correlation function of the AF (thick line) and AD (thin line). Total velocity correlation functions for the (b) ARD, (c) PD, and (d) ID datasets. The dashed lines [in (a) only for AF] denote the 95% CL that is estimated as $2/(n^*)^{1/2}$ (Priestley 1981), where n^* is the number of independent observations and is estimated as $n^* = (\Delta t N_p)/T_L$, where N_p is the number of observations for each dataset.

ance $\sigma_A^2 = (1/2)(\sigma_{a_1}^2 + \sigma_{a_2}^2)$ are computed from the velocity and acceleration time series $u_i(j)$ and $a_i(j)$ as follows:

$$\sigma_{u_i}^2 = \frac{1}{N-2}\sum_{j=1}^{N-1}[u_i(j) - \overline{u}_i]^2 \quad \text{and}$$

$$\sigma_{a_i}^2 = \frac{1}{N-3}\sum_{j=1}^{N-2}[a_i(j) - \overline{a}_i]^2,$$

where $\overline{u_i} = (N-1)^{-1}\Sigma_{j=1}^{N-1}u_i(j)$, $\overline{a_i} = (N-2)^{-1}\Sigma_{j=1}^{N-2}a_i(j)$, and N is the number of points of the trajectory.

We then compute for each trajectory the ratio $y = T_a/T_v$. When $T_L^2 < 4(\sigma_U^2/\sigma_A^2)$ (which is equivalent to $\alpha_1^2 < 4\alpha_2$, in the notation of section 2), we have that T_v, $T_a = a \pm ib \in C$, $|T_v| = |T_a|$, and $|y| = 1$. In this case, the trajectory is characterized by an oscillatory behavior and it is interesting to compute also the dimensionless parameter

TABLE 4. For each dataset: mean values and std dev of T_L, T_v, T_a (expressed in days), y, and eddy kinetic energy ($cm^2\ s^{-2}$). The number in parentheses is the median of the relative PDF.

	T_L	T_v	T_a	y	EKE
AF	5.0 ± 11.2 (4.7)	3.3 ± 11 (2.7)	1.6 ± 1.0 (1.5)	0.7 ± 0.4 (1.0)	89 ± 165 (29)
AD	2.7 ± 1.2 (2.5)	2.3 ± 1.4 (2.0)	0.5 ± 0.3 (0.4)	0.4 ± 0.4 (0.2)	331 ± 467 (183)
ARD	1.9 ± 0.8 (1.7)	1.4 ± 0.9 (1.1)	0.5 ± 0.2 (0.5)	0.6 ± 0.4 (0.5)	163 ± 114 (147)
PD	3.0 ± 1.3 (2.8)	2.6 ± 1.4 (2.4)	0.4 ± 0.3 (0.3)	0.3 ± 0.3 (0.1)	304 ± 366 (194)
ID	2.8 ± 1.3 (2.6)	2.3 ± 1.4 (2.1)	0.5 ± 0.4 (0.4)	0.4 ± 0.4 (0.2)	428 ± 423 (295)

$$x = \frac{b}{a} = \frac{\sqrt{4\frac{\sigma_U^2}{\sigma_A^2} - T_L^2}}{T_L}, \tag{21}$$

which represents the ratio between the oscillatory and memory time scales. It may be analytically shown that when $2\alpha_2 < \alpha_1^2 < 4\alpha_2$ the velocity correlation function (16) oscillates but the corresponding velocity spectrum has no peak. An illustrative example, kindly suggested by an anonymous reviewer, directly shows how the experimental computation of the ratios y and x identifies a looping trajectory. In this case, the Lagrangian velocity components (υ_1, υ_2) may be approximated as

$$\upsilon_1(t) = V\cos(\omega t) \quad \text{and} \quad \upsilon_2(t) = V\sin(\omega t),$$

where V is the constant scalar velocity, $\omega = V/r$ is the angular velocity, and r is the radius of the loop of the trajectory. It can be easily shown that

$$R(\tau) = \cos(\omega\tau),\ T_L = \int_0^{\pi/(2\omega)} \cos(\omega\tau)\, d\tau = \frac{1}{\omega}$$

(in view of the first zero crossing technique),

$$\frac{\sigma_U}{\sigma_a} = \frac{1}{\omega}, \quad \text{and} \quad T_\upsilon,\ T_a = \frac{1}{2\omega}[1 \pm (1-4)^{1/2}].$$

Therefore we have that $|y| = 1$ and $x = (3)^{1/2} > 1$.

From a technical point of view, the computation of T_a and T_υ strongly depends on the interpolation and smoothing procedures applied to the original drifter data. We performed the same analysis presented here without smoothing the data by the boxcar average, and, even if the relative population of the different classes of trajectories is different (see Fig. 7), the overall description and the geographical distribution (see section 4) of the different turbulence regimes are qualitatively similar. Last, we tested the sensitivity of the method on the length of the time series, performing the same analysis using 128-day-long trajectories, and even in this case we found slightly different relative population in each class with unchanged general results.

In Figs. 5, 6, and 7 we show, for the five datasets, the probability density functions (PDF) of the computed values of T_L, T_a, and y; as expected (see also Table 4), the AF dataset shows for T_L, T_a, and y a distribution shifted toward higher values. In Fig. 8 we show, for the drifters and subsurface floats datasets, the scatterplot of the decorrelation length $L_L = \sigma_U T_L$ versus the square root of the eddy kinetic energy σ_U. The black and yellow crosses indicate values of drifters and floats characterized by having $y < 0.2$ and $0.4 < y < 0.8$, and the blue and red crosses are relative to the floats and drifters whose time scales lie in the complex conjugate space with, respectively, $|y| = 1$, $x < 1$, and $|y| = 1$, $x > 1$. For small y, the decorrelation length is approximately linearly dependent on σ_U, whereas when the time scales become complex the dependence on the eddy kinetic energy is definitely weaker and, for large σ_U, L_L is nearly constant.

This simple observation may have important consequences; in fact a qualitative view of the source of the Lagrangian variability may be obtained considering the two limiting cases in which the Eulerian field evolves slowly ($\sigma_U \gg L_E/T_E$, strong spatial structure or frozen turbulence regime) or rapidly ($\sigma_U \ll L_E/T_E$, weak spatial structure or fixed-float regime), where $c_* = L_E/T_E$ is the evolution speed of the eddy field (Lumpkin et al. 2002) and T_E and L_E are the Eulerian counterparts of T_L and L_L.

In the frozen turbulence regime, the Lagrangian decorrelation is determined by the space variability of the Eulerian field, and

$$L_L \sim L_E \ll \sigma_U T_E \quad \text{and} \quad T_L \sim L_L/\sigma_U \ll T_E. \tag{22}$$

In the fixed-float regime, the float/drifter samples mesoscale fluctuations like a current meter and the Lagrangian decorrelation is determined by the time variability of the Eulerian velocity field; consequently one has

$$T_L \sim T_E \quad \text{and} \quad L_L \sim \sigma_U T_E \ll L_E. \tag{23}$$

In the fixed-float regime, assuming a constant Eulerian time scale, $L_L \propto \sigma_U$, and the Eulerian and Lagrangian time statistical properties are similar, while in the frozen turbulence $L_L \sim L_E$ and the frequency Lagrangian energy spectrum tends to the wavenumber Eulerian energy spectrum (Middleton 1985).

Even if the clear predominance of one of the two limiting cases is not observed in the real ocean, it is interesting to note their implications. Firstly, if the oceanic velocity field was uniformly in a fixed-float, or frozen field regime it could be possible to use the more accessible Eulerian scales (time and space, respectively) as a proxy for Lagrangian scales. Secondly, if the Eulerian field selects the time and space scales independently of the kinetic energy we have that in the frozen field

$$L_L \sim L_E \sim \text{const} \quad \text{and} \quad K \sim \sigma_U^2 T_L = \sigma_U L_L \propto \sigma_U, \tag{24}$$

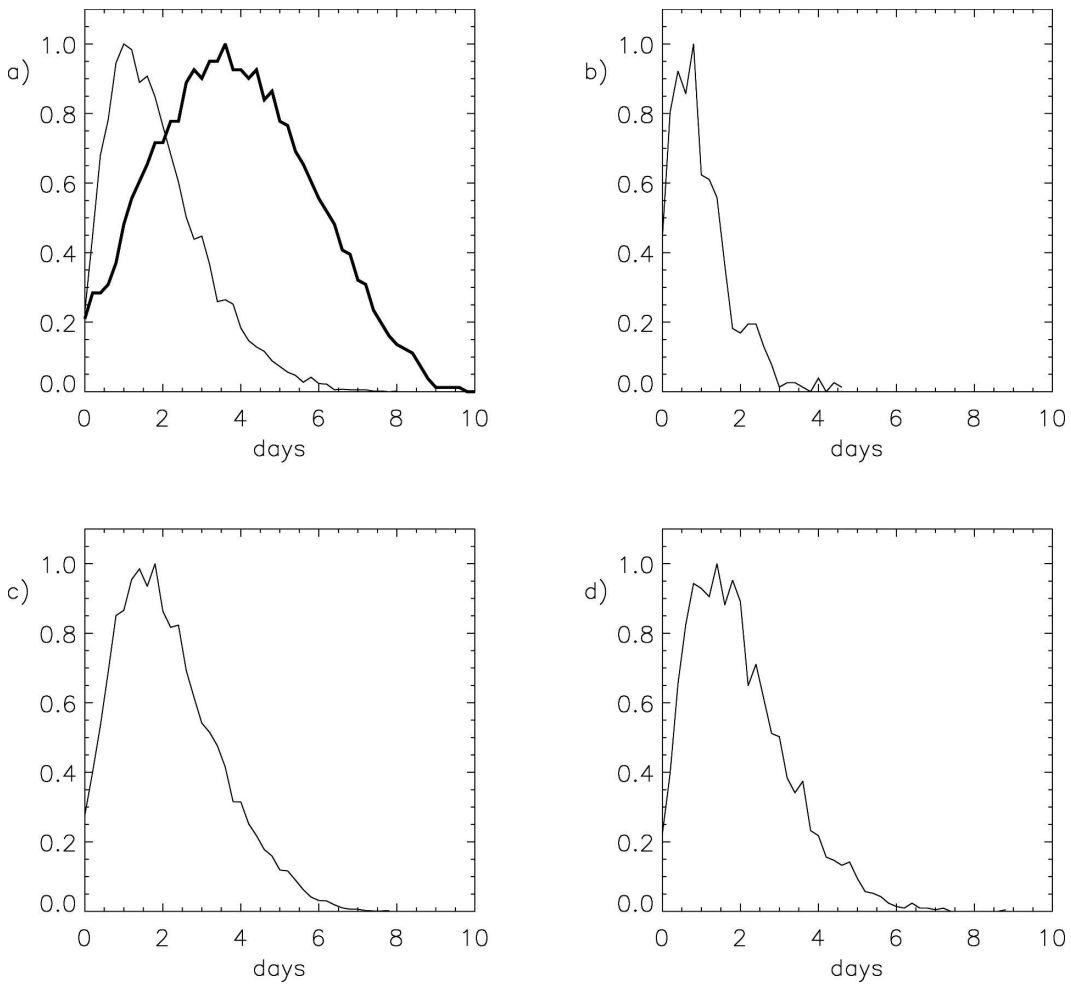

FIG. 5. Probability distribution function of the estimated values of T_L for the (a) AF and AD datasets (thick and thin line) and for the (b) ARD, (c) PD, and (d) ID datasets.

while in the fixed-float regime

$$T_L \sim T_E \sim \text{const} \quad \text{and} \quad K \sim \sigma_U^2 T_L \propto \sigma_U^2. \quad (25)$$

We know that the Eulerian length scales vary as a function of latitude from about 100 km at 50°N/S to greater than 160 km within 8° of the equator (e.g., Stammer 1997). The behavior stated by (24) and (23) essentially is that, at a given latitude, variations of L_L are primarily due to changes in turbulence regimes and not to variations of L_E.

Middleton (1985), studying different experimental datasets, has shown that the case $T_L/T_E < 1$ [(22)] is the most generic one; more recently Lumpkin et al. (2002), analyzing experimental and numerical data in the North Atlantic, have shown that neither a fixed-float or frozen field regime characterizes the full set of observations. Nevertheless, results shown in the same paper as well as several other regional studies (Rossby et al. 1983; Krauss and Böning 1987; Poulain and Niiler 1989; Figueroa and Olson 1989; Brink et al. 1991) indicate that for energetic mesoscale flows, the regime (22) with $L_L \sim$ const and $K \propto \sigma_U$ seems to be the most appropriate. Hua et al. (1998), by means of numerical experiments, found that also the geostrophic turbulence seems to be more consistent with the frozen turbulence regime.

Based upon these considerations, we think that the plot of Fig. 8 shows that the ratio $y = T_a/T_v$ can be considered as a useful index to discriminate between the frozen turbulence and fixed-float regime. Moreover, plotting the mean position of the trajectories belonging to the different classes (plot not shown here) it is possible to see that the trajectories that have complex conjugates time scales are mainly located in the regions characterized by strong currents.

To get a direct feeling about the qualitative differ-

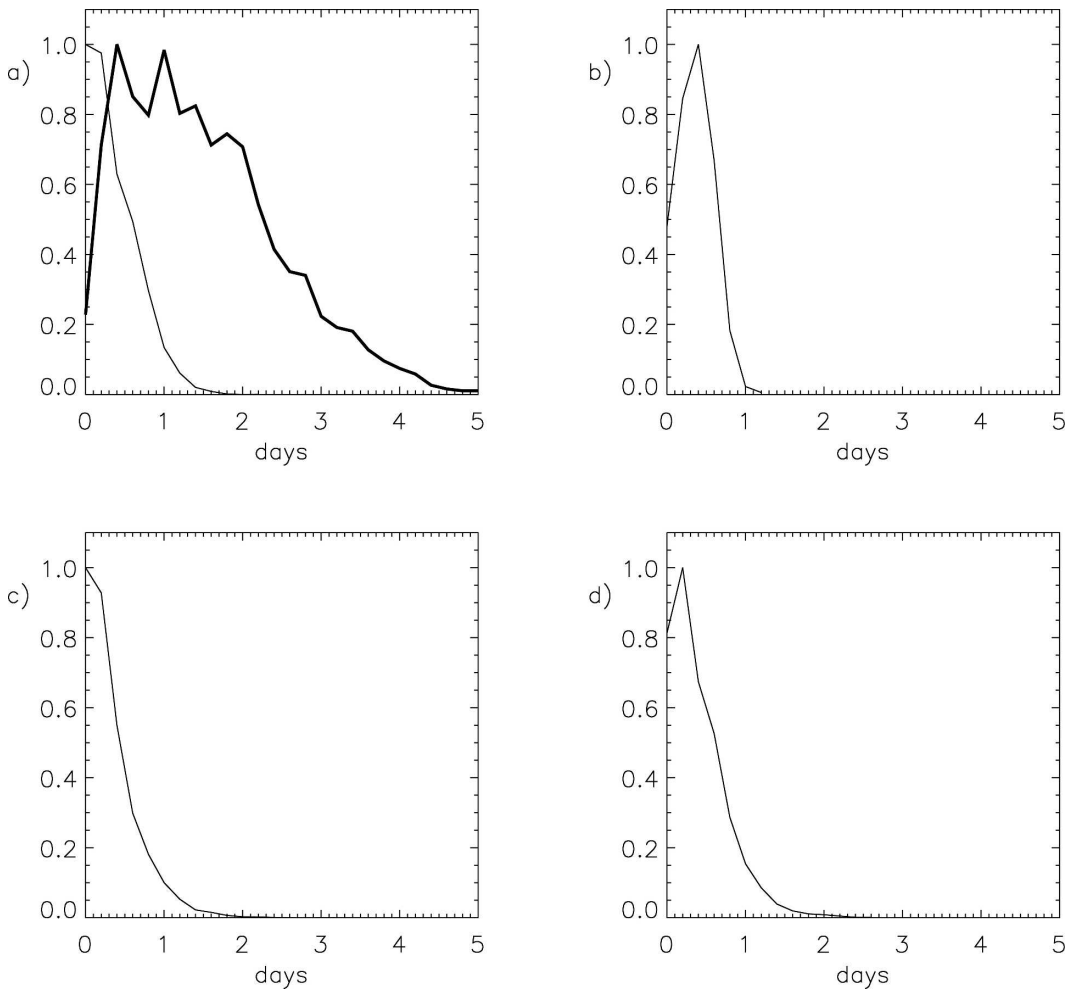

FIG. 6. Probability distribution function of the estimated values of T_a for the (a) AF and AD datasets (thick and thin line) and for the (b) ARD, (c) PD, and (d) ID datasets.

ence between trajectories characterized by different values of the ratio $y = T_a/T_v$, we plot in Figs. 9–11 (only for AF, AD, and PD) typical trajectories of the four classes defined by $y < 0.2$ (class I), $0.4 < y < 0.8$ (class II), $|y| = 1$ $x < 1$ (class III), and $|y| = 1$ $x > 1$ (class IV). Trajectories belonging to the two extreme classes I and IV are considerably different. In class I, there are grouped floats and drifters characterized by large-scale meandering influenced by high-frequency variability. In class IV, trajectories are clearly influenced by the presence of coherent structures and very often they rapidly whirl, trapped inside an eddy with a well-defined length scale (looping behavior). This is partly true also for the trajectories characterized by $|y| = 1$ and $x < 1$ (class III), even if in this case the length scale of the loops is not well defined and often the floats/drifters seem to jump between eddies of different size. Last, floats/drifters of the class II ($0.4 < y < 0.8$) have trajectories showing intermediate characteristics and, meandering around large-scale structures, they did not show a clear influence of high-frequency motions.

In the presence of coherent structures only particles trapped in the eddies quickly rotate, while the rest of the particles meander in the less energetic turbulent background experiencing only sporadic looping behavior. Richardson (1993) has introduced the simple criterion of defining a looper as a trajectory that undergoes at least two consecutive loops in the same direction. Veneziani et al. (2004), analyzing subsurface floats in the northwest Atlantic, found that in this area the percentage of looping floats varies from 15% to 40%.

Even if an exhaustive analysis is difficult, because of the huge number (25 091) of trajectories analyzed in this work, we believe that the method proposed here, and based on the computation of the ratio $y = T_a/T_v$, is

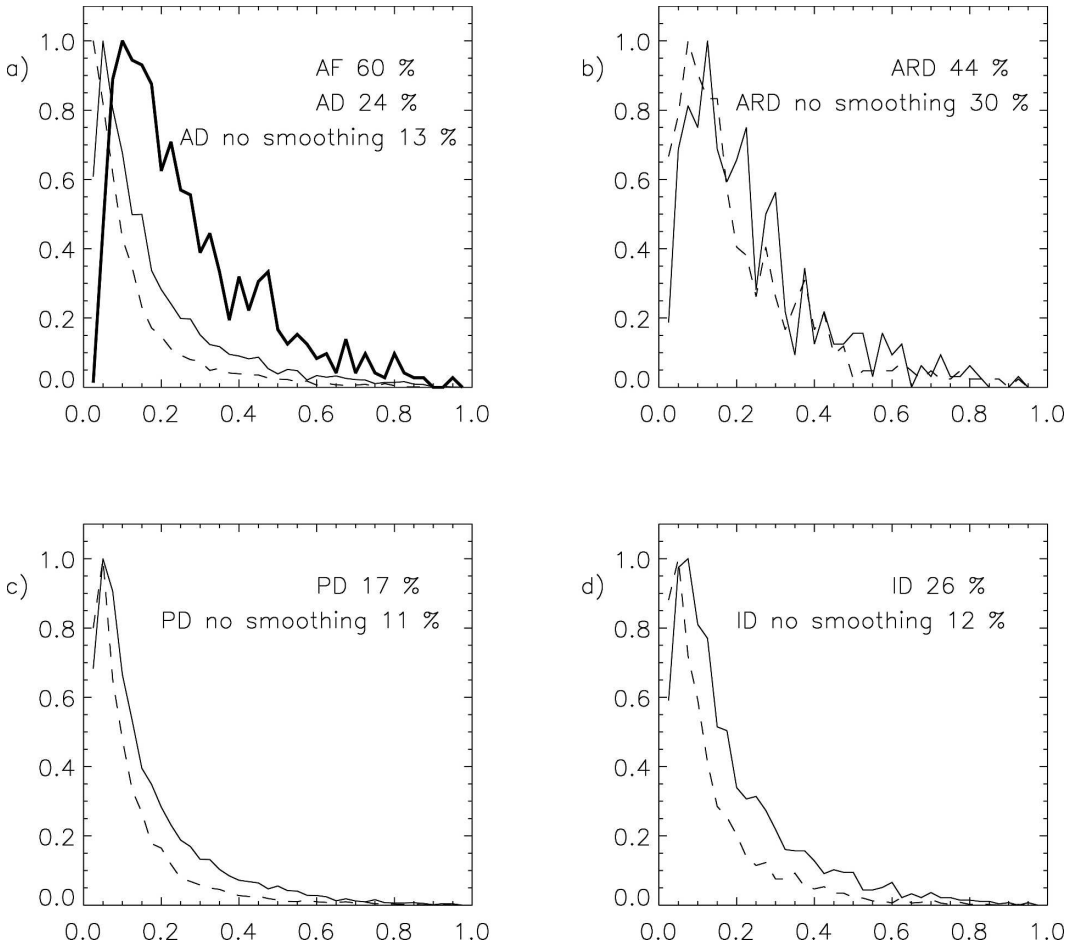

FIG. 7. Probability distribution function of the estimated values of $y = T_a/T_v$ for (a) the AF and AD datasets (thick and thin line) and for the (b) ARD, (c) PD, and (d) ID datasets. The dashed lines represent the PDF of y obtained without smoothing the drifter trajectories with the boxcar average described in section 3. The number on the top represents the percentage of trajectories having complex conjugates time scales (classes III and IV). For the surface drifters we report also the percentage computed without smoothing the original trajectories.

capable of identifying looping trajectories. An inventory (postscript file) of all the trajectories analyzed here divided per classes was available at http://clima.casaccia.enea.it/staff/rupolo/trajectorybook/index.html.

In the following we will designate as turbulent the trajectories belonging to classes III and IV that, coherent with previous observations (e.g., Krauss and Böning 1987) and results from 2D turbulence studies (e.g., Babiano et al. 1987; Pasquero et al. 2001), are characterized by smaller correlation times and greater energetic contents (see Tables 5 and 6).

It is crucial to note the different relative importance (Table 7) of these classes in the five datasets. While in AF more than one-half of the trajectories (60%) belong to the turbulent classes III and IV, in the main world's ocean basins (AD, PD, and ID) the surface trajectories are mainly influenced by high-frequency motions (class I) and the percentage of turbulent trajectories (classes III and IV) vary from a minimum of 17% (PD) to a maximum of 44% (ARD), the most turbulent surface dataset. The same relative importance, with different values of percentage, it is observed when analyzing drifter data without the boxcar smoothing procedure, as it is possible to see in Fig. 7 where are reported the percentages of drifters belonging to classes III and IV.

The capability of the proposed method of separating the whole dataset in more homogeneous classes is also evident from Fig. 12, where we plot for the five datasets the correlation functions of each class with the time axis normalized by T_L. Correlation functions of the same class, but that belong to different ocean basins, display very similar shapes, while correlation functions of the different classes are characterized by qualitatively dissimilar time behavior. In particular, it is worth noting

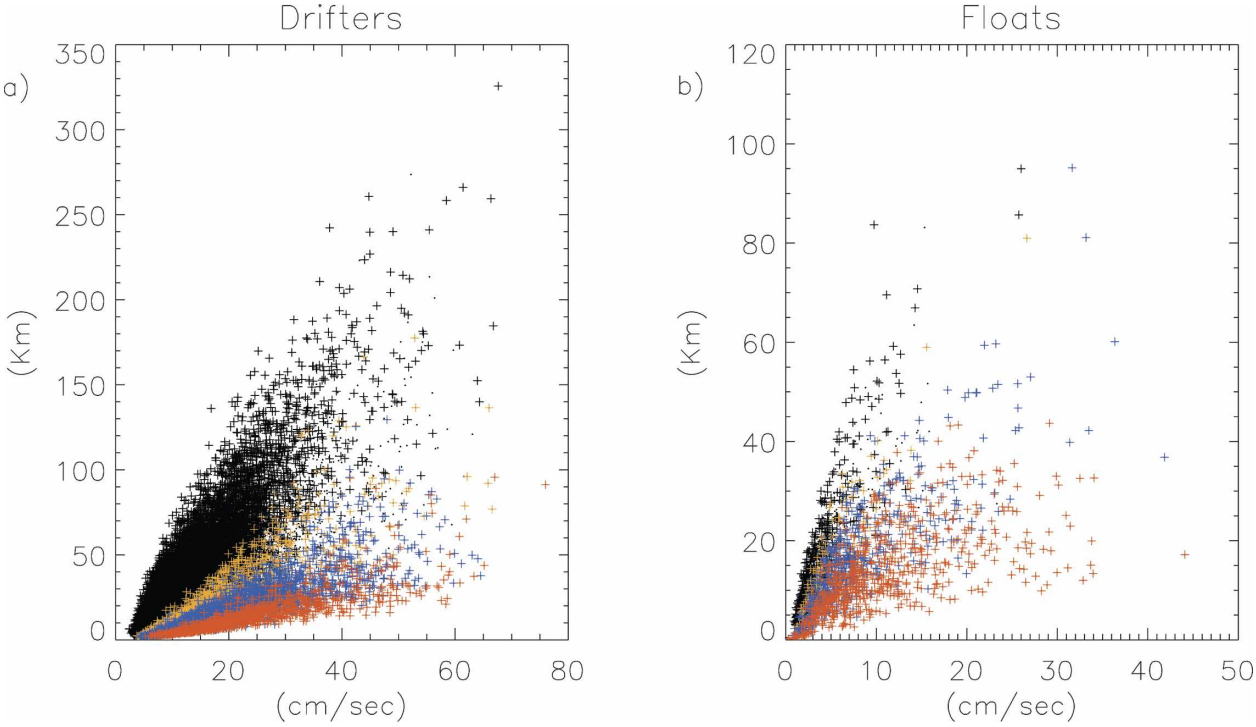

FIG. 8. Scatterplot of L_L vs σ_U for the (left) surface drifters and (right) subsurface floats datasets. The black, yellow, blue, and red crosses are related to floats and drifters with $y < 0.2$, $0.4 < y < 0.8$, $|y| = 1$, $x < 1$, and $|y| = 1$, $x > 1$, respectively.

the clear oscillations in the class IV (red curves in Fig. 12) and the smooth behavior for $t \sim 0$ for the classes II, III, and IV, as expected for trajectories characterized by a finite variance of the acceleration. Looking in more detail, we may also notice that there are minor differences between the different datasets (as the great negative lobe for the velocity correlation functions of class I of AF) and discrepancies between the expected theoretical behavior and the computed normalized velocity correlation functions, as, for example, the weak oscillatory behavior for functions belonging to class III. This is not surprising since the analysis is based upon the estimate of the Lagrangian time scale directly from the single trajectory, through the first zero crossing technique. Nevertheless, the qualitative behavior of the dimensionless single-particle dispersion, that is obtained integrating the Taylor relation (5) without the dimensional value σ_U^2 and rescaling time by T_L, is similar in the different datasets. In Fig. 12f we plot this function only for the AD dataset; this figure shows that the influence of the coherent structures (classes IV and III, red and blue lines) appears to be more important only for times smaller than ~ 4–$5T_L$. It is also interesting to note that for larger times only the single-particle dispersion of class IV clearly exhibits the transition from ballistic motion to the random walk regime, which is also found in 2D turbulence simulations (Babiano et al. 1987; Pasquero et al. 2001).

Quantitative information on the real dispersal properties is given by the dimensional single particle that obviously depends both on the kinetic energy and on the relative population of each class that, as it will be discussed in the next section, strongly varies in the geographical space and in the different current systems.

In a recent paper Veneziani et al. (2004) propose a quantitative criterion to define looping trajectories, based on the computation, for each trajectory, of the mean angular velocity Ω. Trajectories are classified as loopers when Ω exceeds a given threshold value ($|\Omega| > 0.1$ days^{-1}). This criterion, applied to the subsurface floats in the northwestern Atlantic, give similar results in terms of number of looper floats. They then interpret the results in terms of a 2D first-order model with spin [formally equivalent to a 1D second-order model (Reynolds 2002)] in which the two characteristic time scales (T_L and $|\Omega|^{-1}$) are formally independent and the Lagrangian motion is due to a superimposition of a correlated noise and a spiraling component. As a contrast, the 1D second-order model presented here allows for a continuous transition from a situation characterized by correlated noise to looping trajectories. An-

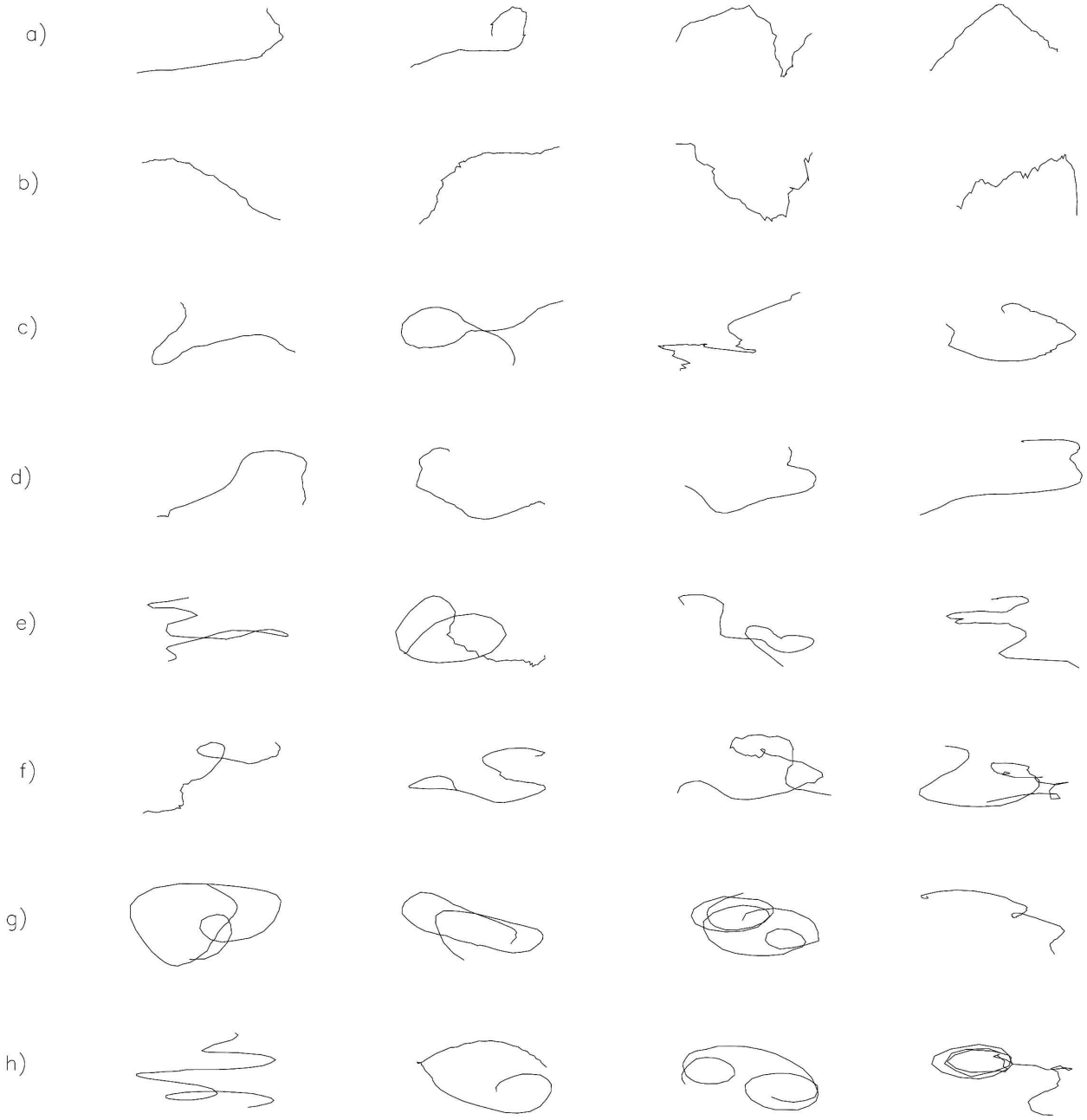

FIG. 9. The AF dataset. Typical trajectories belonging to (a), (b) class I ($y < 0.2$), (c), (d) class II ($0.4 < y < 0.8$), (e), (f) class III ($|y| = 1$, $x < 1$), and (g), (h) class IV ($|y = 1$, $x > 1$). The plot is rescaled using the maximal extension in the zonal (abscissa) and meridional (ordinate) directions.

other difference consists in the fact that directly computing Ω it is possible to distinguish cyclonic and anticyclonic loopers. Since both criteria need to estimate the derivative of the velocity, they are probably characterized by similar uncertainties, because of technical difficulties in determining the right smoothing procedure of the original trajectory. We think that a comparison of these two screening criteria could be of interest, and we believe that besides the limitation given by the difficult estimate of the time scales, the coherence of the results presented here confirms the validity also of the approach based upon the screening of the trajectories by means of the dimensionless index $y = T_a/T_v$. In the next section, we will exploit these results to characterize the main oceanic current systems in terms of turbulence regimes.

FIG. 10. As in Fig. 9, but for dataset AD.

4. Dispersal properties and turbulence regimes in the main oceanic currents

Until now, all the analyses were performed carrying out means on quasi-homogeneous trajectories covering huge geographical areas. In this section we will study the main oceanic current systems mapping on the geographical space parameters computed from the trajectories. All these maps are obtained by averaging, on a grid of $1° \times 1°$, between all the points falling in a given bin, and assigning to each point, the trajectory value. This technique, which was already used by Lumpkin et al. (2002) and partly tested by Berloff et al. (2000), allows us to maximize the amount of data and to map quantities computed along the entire trajectory (as correlation parameters). On the other hand, the nonlocal-

FIG. 11. As in Fig. 9, but for dataset PD.

TABLE 5. Mean value and std dev of the correlation time T_L (days) of the different classes of trajectories of the five datasets.

	Class I $y < 0.2$	Class II $0.4 < y < 0.8$	Class III $\|y\| = 1$, $x < 1$	Class IV $\|y\| = 1$, $x > 1$
AF	7.1 ± 24.6	5.5 ± 1.7	5.0 ± 1.8	3.3 ± 1.5
AD	3.4 ± 1.2	2.1 ± 0.6	1.8 ± 0.5	1.2 ± 0.2
ARD	2.7 ± 0.9	1.7 ± 0.4	1.4 ± 0.3	1.1 ± 0.2
PD	3.5 ± 1.2	2.3 ± 0.8	1.9 ± 0.7	1.3 ± 0.2
ID	3.5 ± 1.2	2.4 ± 0.9	1.9 ± 0.7	1.4 ± 0.5

TABLE 6. Mean value and std dev of the eddy kinetic energy σ_U^2 (cm^2 s^{-2}) of the different classes of trajectories of the five datasets.

	Class I $y < 0.2$	Class II $0.4 < y < 0.8$	Class III $\|y\| = 1$, $x < 1$	Class IV $\|y\| = 1$, $x > 1$
AF	24 ± 55	36 ± 67	89 ± 164	164 ± 220
AD	198 ± 310	414 ± 557	511 ± 538	830 ± 703
ARD	140 ± 134	173 ± 95	165 ± 100	212 ± 106
PD	233 ± 267	370 ± 362	441 ± 443	579 ± 776
ID	297 ± 288	514 ± 429	580 ± 473	868 ± 700

ity of the considered values can affect the results in case of trajectories spanning a very large geographical area.[1]

The geographical distribution of the Lagrangian eddy kinetic energy (EKE) at surface (Fig. 13a) highlights, similar to previously published results (e.g., Stammer 1997; Lumpkin et al. 2002), many of the main oceanic currents: the equatorial bands, the Gulf Stream and North Atlantic Current systems (GS/NAC), the Loop Current in the Gulf of Mexico, the Agulhas retroflection area and the Brazil–Malvinas confluence in the Atlantic Ocean; the Mozambique-Agulhas and the Leuuwin currents in the Indian Ocean; the Kuroshio and the East Australia Current (EAC) together with the area west of Central America in the Pacific. However, other important current systems do not show high values of EKE as, for example, the Antarctic Circumpolar Current (ACC), which is only partly marked by high values of EKE, or the North Equatorial Current at around 10°N in the western Pacific, which is even characterized by a minimum of EKE (Zhurbas and Oh 2004), because of their strong component of the mean zonal flow. At subsurface in the Atlantic (Fig. 13 b) the Gulf Stream, the Agulhas retroflection and the Brazil–Malvinas confluence areas are clearly evident.

The geographical distribution of T_L (Fig. 14) shows a general tendency, both at surface and subsurface, to have larger values in the less energetic interior of the oceans in opposition to the energetic currents that are characterized by shorter decorrelation velocity time scales (the opposite is true for the acceleration time scale, map not shown here). Some energetic areas, such as the GS, the EAC, the Loop Current, the Agulhas system and the Brazil–Malvinas confluence, are clearly marked by relative minima of T_L. However, it is interesting to note that this general tendency it is not observed in the equatorial bands and is less evident in the Kuroshio Current [the same result was obtained by Stammer (1997)]. At surface the Lagrangian correlation length (map not shown) is less than 50–60 km almost everywhere, except in the Kuroshio region and in the tropical bands, where it reaches values greater than 100 km; in the energetic regions marked by a relative minimum of T_L the Lagrangian correlation is only slightly greater than the background value.

The geographical distribution of the ratio $y = T_a/T_v$ shows that the subsurface AF dataset (Fig. 15b) is the most homogeneous and is characterized by a mean value of y that is relatively large everywhere. The highest values of $y = T_a/T_v$ (>0.8) are observed in the GS/NAC and Agulhas retroflection area, in the Brazil–Malvinas Current and, not uniformly, in the Mediterranean outflow area. With the exception of this latter area, the same regions are evidenced in the surface AD dataset (Fig. 15a), where high values of y are observed also between the NAC and Azores Current, in the Norwegian Current, in the Gulf of Mexico, in the central equatorial band and near the northern coasts of South America.

At the surface of the Pacific Ocean, one can distinguish, in a more quiescent background, the turbulent areas east of New Guinea, where the westward flow of

[1] An alternative approach consists in binning Lagrangian velocities in the physical space and then to compute statistics in the obtained Eulerian map. In this case, when dealing with time correlation properties, one has first to compute a mean correlation function and then to estimate a single correlation time for the entire area.

TABLE 7. Mean values and std dev of y (classes I and II) and x (classes III and IV), number of trajectories, and relative percentage for each class of the five datasets.

	Class I $y < 0.2$	Class II $0.4 < y < 0.8$	Class III $\|y\| = 1$, $x < 1$	Class IV $\|y\| = 1$, $x > 1$
AF	(y) 0.11 ± 0.05, 413, 20%	(y) 0.5 ± 0.1, 151, 7%	(x) 0.6 ± 0.2, 603, 29%	(x) 1.4 ± 0.3, 645, 31%
AD	(y) 0.08 ± 0.05, 3976, 54%	(y) 0.5 ± 0.1, 508, 7%	(x) 0.6 ± 0.2, 1310, 18%	(x) 1.2 ± 0.2, 448, 6%
ARD	(y) 0.11 ± 0.05, 160, 29%	(y) 0.5 ± 0.1, 49, 9%	(x) 0.6 ± 0.2, 163, 29%	(x) 1.2 ± 0.1, 84, 15%
PD	(y) 0.08 ± 0.05, 7441, 61%	(y) 0.5 ± 0.1, 784, 6%	(x) 0.6 ± 0.2, 1575, 13%	(x) 1.3 ± 0.2, 461, 4%
ID	(y) 0.09 ± 0.05, 1479, 50%	(y) 0.5 ± 0.1, 216, 7%	(x) 0.6 ± 0.2, 598, 20%	(x) 1.2 ± 0.2, 170, 6%

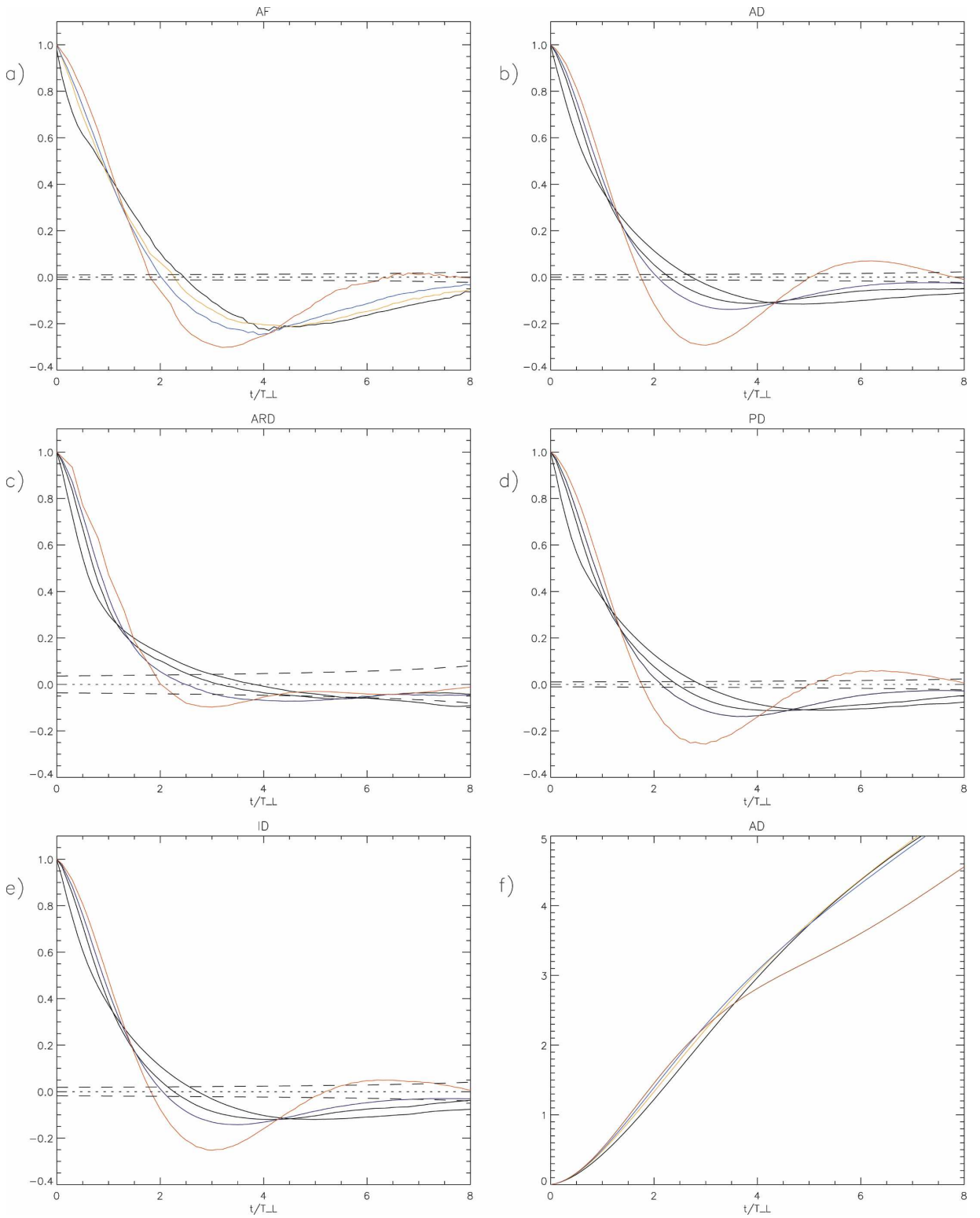

FIG. 12. Total velocity correlation functions vs time with the time axis normalized by T_L for (a) AF, (b) AD, (c) PD, (d) ARD, and (e) ID datasets. The zero value is indicated by dotted lines. The dashed lines denote the 95% CL (only for class IV) that is estimated as in Fig. 4. (f) Plotted are the normalized single-particle dispersion for the four classes of trajectories for the AD dataset. In each plot the black and the yellow lines refer to floats/drifters belonging to classes I and II ($y < 0.2$, and $0.4 < y < 0.8$), while the blue and red lines refer to floats/drifters belonging to classes III and IV ($|y| = 1$, $x < 1$ and $|y| = 1$, $x > 1$), respectively.

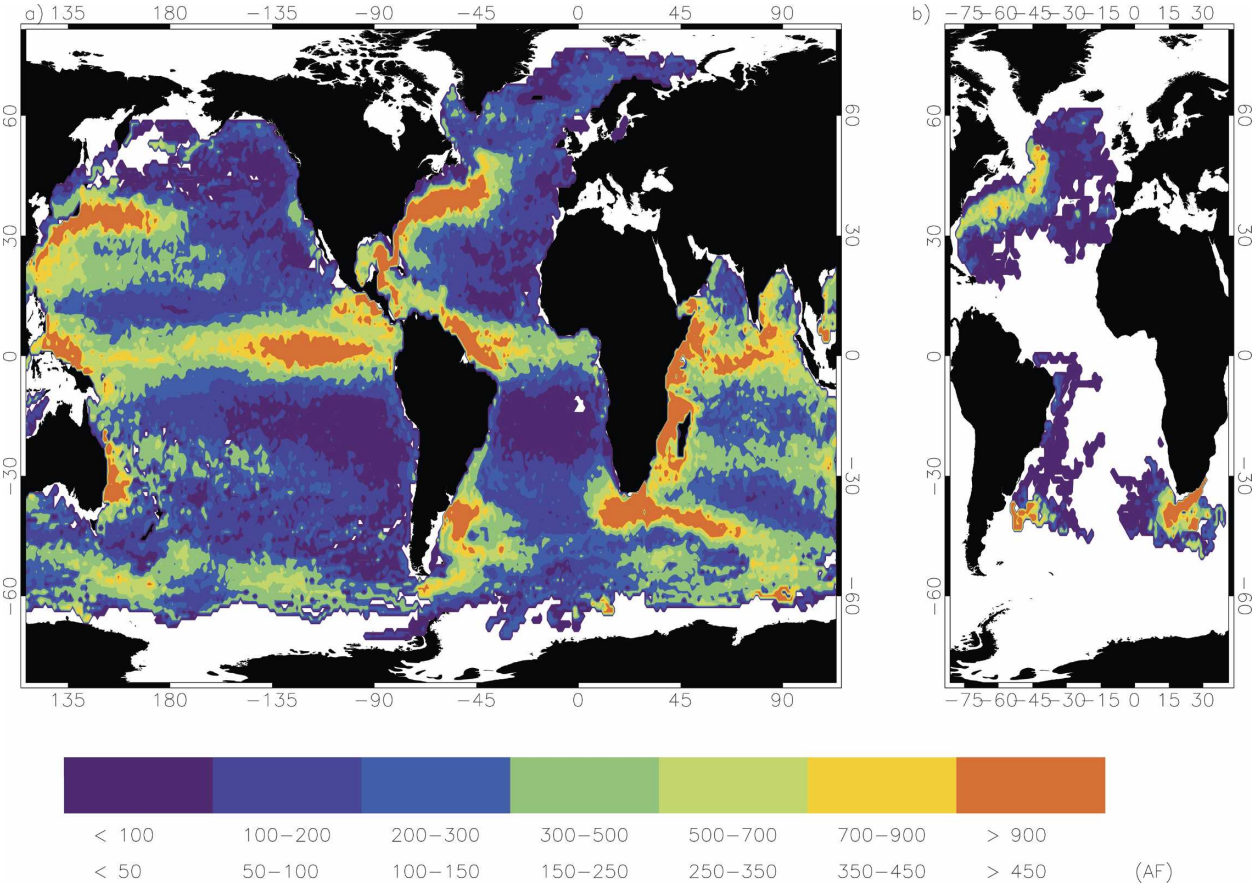

FIG. 13. Maps of the Lagrangian EKE ($cm^2\ s^{-2}$) for (a) the surface drifters and (b) the subsurface Atlantic floats. The upper (lower) numbers in the color scale refer to the surface drifters (subsurface floats) dataset.

the South Equatorial Current (SEC) turns to the north and east to feed the North Equatorial Counter Current (NECC), east of Australia (EAC), and west of Mexico. Moreover, it is possible to observe a large tongue with intermediate values of y within 20°–30°N southeast of the Kuroshio area, linked to the baroclinic instabilities in the seasonal North Subtropical Counter Current (NSTCC); a less-prominent counterpart it is observed also in the South Pacific where a strong seasonal signal is also observed (Zhurbas and Oh 2004).

In the Indian Ocean, relatively high values of y are observed along the eastern coasts of the Peninsula Arabica and of Africa till the Mozambique–Agulhas system, in the equatorial band and in the Leuuwin current west of Australia. Last, the few drifters in the ACC are characterized by relatively high values of y.

Even if the finite time and space scales of ocean variability do not support the eddy diffusivity model (e.g., Davis 1987) and the Lagrangian diffusivity is not defined if the velocity spectrum does not saturate at low frequencies, the use of an eddy diffusivity model is common in OGCMs. In recent years, efforts have been devoted to calculate lateral diffusivity from Lagrangian data, or directly from the Taylor relation (5) or following other approaches (e.g., Griffa et al. 1995; Davis 1987, 1991; Oh et al. 2000; for a review see Zhurbas and Oh 2003). The interest of this kind of study relies mainly in the investigation of possible relationship between diffusivity and kinematic or dynamical quantities, since in the OGCMs the actual value of the eddy diffusivity depends on many technical details and above all on the grid space resolution. Consequently, to characterize the different oceanic currents in terms of diffusivity, we simply map in Fig. 16 the quantity $\Gamma = \sigma_U^2 T_L = \sigma_U L_L$ that has to be considered as a, dimensionally homogeneous, proxy (Stammer 1998; Lumpkin et al. 2002) of the Lagrangian eddy diffusivity K defined in section 2.

The surface Γ field shown in Fig. 16 is very similar to the diffusivity field estimated by Zhurbas and Oh (2004) using a different approach (Zhurbas and Oh 2003). The maximum values of Γ presented here

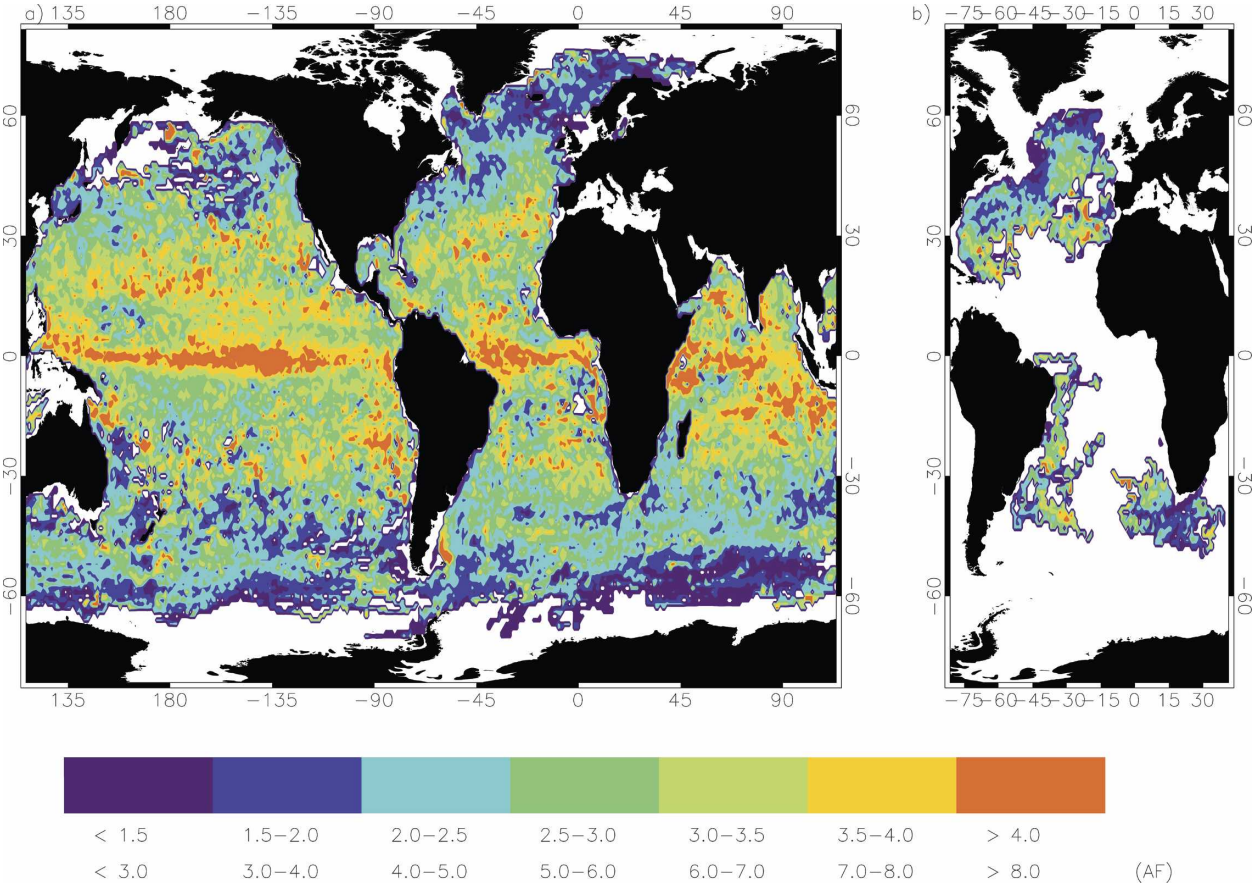

FIG. 14. Maps of the Lagrangian correlation time T_L, expressed in days, for (a) the surface drifters and (b) the subsurface Atlantic floats. The upper (lower) numbers in the color scale refer to the surface drifters (subsurface floats) dataset.

slightly exceed the maximum values of their estimate but the overall paths coincide. The only worth noting difference is that in their analysis is less evident the suppressed rate of diffusivity (discussed below) in the areas characterized by the presence of coherent structures.

At surface, Γ is higher in the main energetic current paths but, consistently with the previous results, the maximum values are observed in the area characterized by high energy and intermediate and low values of y, such as the Kuroshio region and the equatorial area. On the contrary, where turbulent trajectories are predominant, as for instance east of Australia or in the Malvinas–Brazil confluence, the same energetic content gives rise to a lower value of Γ.

In the Pacific, the NEC is characterized by a minimum of Γ that shows a general tendency to increase westward (eastward) in the midlatitudes (equatorial regions) and toward the equator in both hemispheres. The highest values are observed in the eastern equatorial Pacific and the lowest ones in the northeast Pacific, northward to the subpolar front and in the eastern subtropics in the South Pacific. In the Atlantic, the main energetic systems are characterized by relative maxima of Γ both at surface and subsurface (Fig. 16b), while in the Indian Ocean maximum values are found in the eastern equatorial regions and in the western boundary currents along the African coasts.

5. Summary and discussion

In this work, we have shown that in many oceanic current systems, both at subsurface and at surface, the Lagrangian motion is characterized by having a nonnegligible (with regard to the observational time sampling) acceleration time scale T_a that may also assume values similar to the velocity time scale T_v. Moreover, we proposed the use of the ratio $y = T_a/T_v$ to rationalize the analysis of huge Lagrangian dataset. In particular, when analyzing the GDP surface dataset and WOCE subsurface floats in the Atlantic, it was shown that trajectories having different values of y are characterized

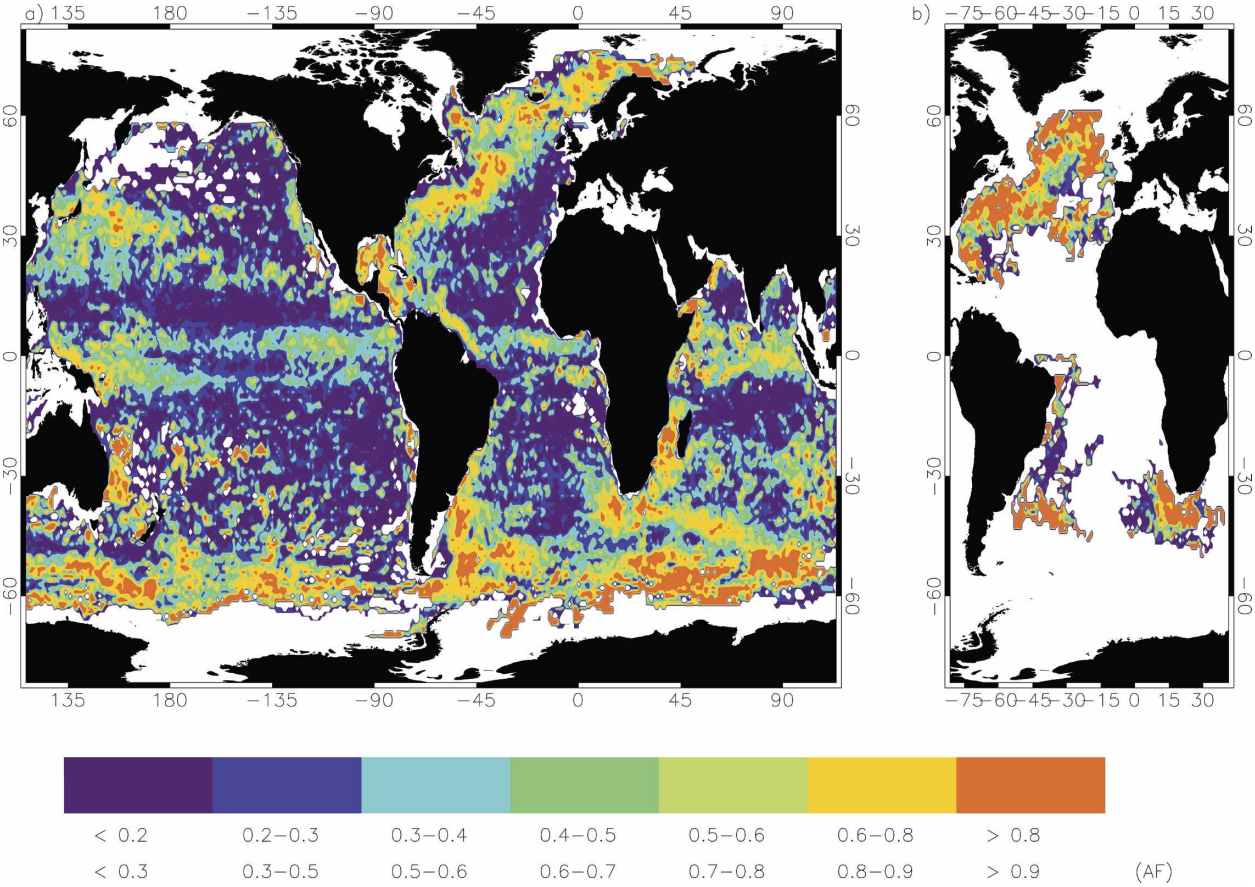

FIG. 15. Maps of the ratio $y = T_a/T_v$ for (a) the surface drifters and (b) the subsurface Atlantic floats. The upper (lower) numbers in the color scale refer to the surface drifters (subsurface floats) dataset.

by different shapes, correlation and dispersal properties. This simple observation has lead to a first characterization of the dispersal properties in the main oceanic current systems.

The subsurface AF dataset is characterized by the highest values of the ratio $y = T_a/T_v$ and by having minimal values of T_L in the most turbulent and energetic areas (Gulf Stream, the Brazil–Malvinas confluence, and in the Agulhas retroflection). At surface, the less-energetic inner oceans are generally characterized by low values of $y = T_a/T_v$ and by mostly constant value of T_L.

Otherwise, the main energetic surface systems in the World Ocean basins can be divided in two categories. The first is characterized by a Lagrangian correlation time decreasing with the eddy kinetic energy and is massively populated by turbulent trajectories. To this category belong the Gulf Stream, Agulhas–Mozambique and the currents east and west of Australia, the Gulf of Mexico and the region west of Mexico. The second is characterized by a Lagrangian correlation length increasing with the eddy kinetic energy and is populated by trajectories having a relatively low value of the ratio $y = T_a/T_v$. The energetic equatorial bands and partly the Kuroshio current belong to this category.

The analysis performed in the previous sections indicates that in the first category the frozen-turbulence regime prevails, and in the second one the fixed-float regime prevails. This kind of a geographical characterization of the main oceanic currents can be useful to advance the representation of the eddy diffusivity in the OGCMs because, in these two regimes, the Lagrangian diffusivity varies differently according to the Lagrangian eddy kinetic energy.

In recent years, a large effort has been devoted by the scientific community to improve the parameterization of eddy diffusivity. This effort was mainly focused on the attempt of mimicking, in coarse resolution models, the effect of baroclinic instability by means of a diffusion coefficient (or an eddy-induced velocity) proportional to some index representative of the isopycnal

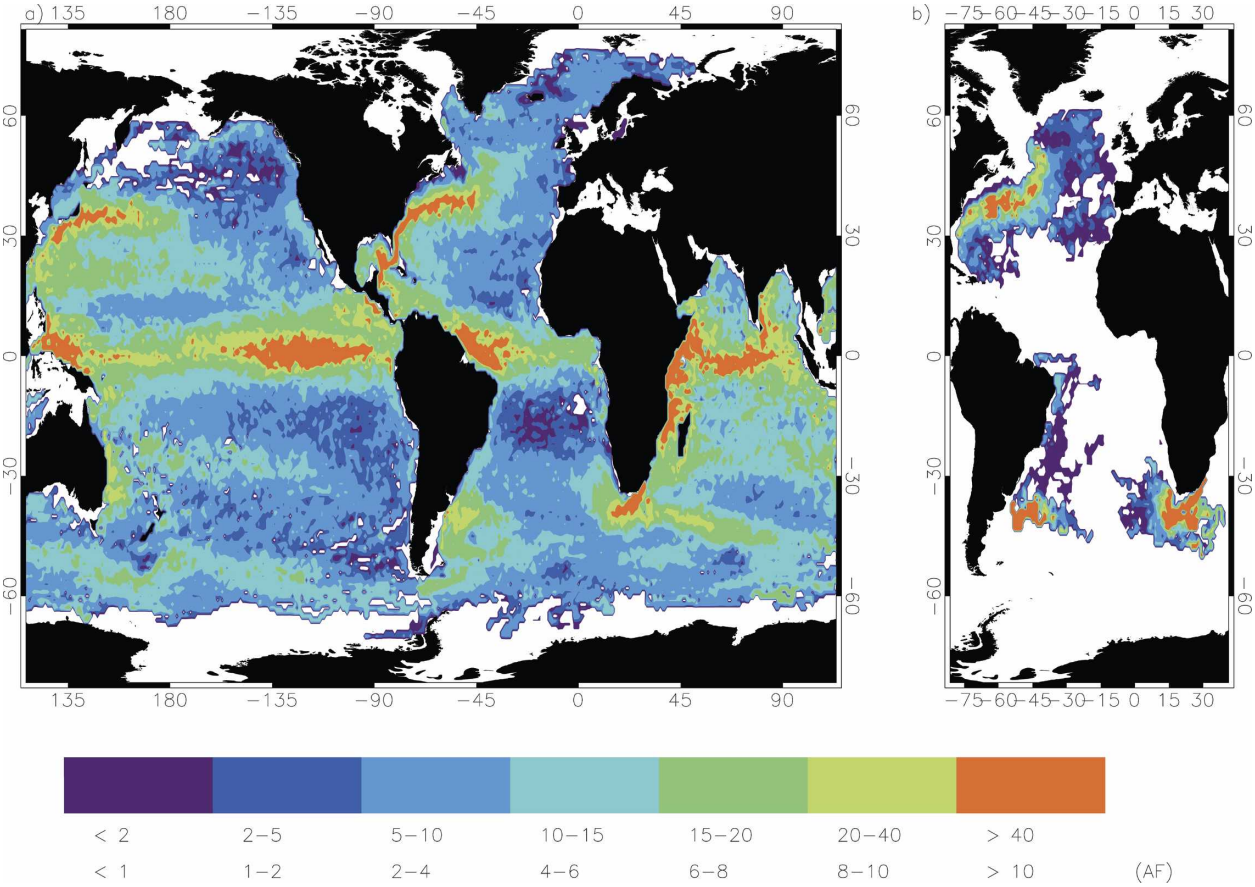

FIG. 16. Maps of the proxy of diffusivity $\Gamma = \sigma_U^2 T_L$ for (a) the surface drifters and (b) the subsurface Atlantic floats. The upper (lower) numbers in the color scale refer to the surface drifters (subsurface floats) dataset (10^7 cm^2 s^{-2}).

slope. The justification for this approach is that baroclinic instability is the main mechanism of energy extraction and is the primary source of eddies (e.g., Treguier et al. 1997; Visbeck et al. 1997; Bryan et al. 1999). Nevertheless, in the oceans exist also regions characterized by large-eddy activity in the absence of strong density gradients. Stammer (1997) has shown (with hydrological and altimeter data) that in the vicinity of the East Australia Current, in the Brazil–Malvinas confluence and in the Agulhas Retroflection, a strong eddy field is present even in absence of important horizontal density gradients. This suggests that the scenario in which the source of eddies is the kinetic, rather than the potential, energy cannot be totally neglected, and that a complete parameterization of eddies should take into account complementary approaches. For instance, McWilliams and Gent (1994) using a double-gyre GCM proposed diffusivity to be proportional to the local kinetic energy times a tapering time dimensional factor, with prescribed spatial form, to avoid an overestimate of diffusivity in the energetic border currents. In the present work, we found strong indications that in the regions evidenced in the analysis of Stammer (1997) and in most of the western boundary currents the Lagrangian diffusivity is proportional to the square root of the eddy kinetic energy. This shows how Lagrangian data, that directly record both kinetic energy and the existence of eddies, may help to indicate in which geographical area a particular parameterization is appropriate.

As an example of this method, we mention the parameterization of the eddy diffusivity proposed by Babiano et al. (1987) that does not account for the contribution of baroclinic instability to the diffusivity fields but describes nonlocal effects of geostrophic turbulence. Such parameterization has been implemented on a regional OGCM by Rupolo et al. (2003) and results into a scaling of the eddy diffusivity coefficient with the square root of the eddy kinetic energy (Fig. 17). We think that the results discussed in this work suggest where it could be useful to improve OGCM results.

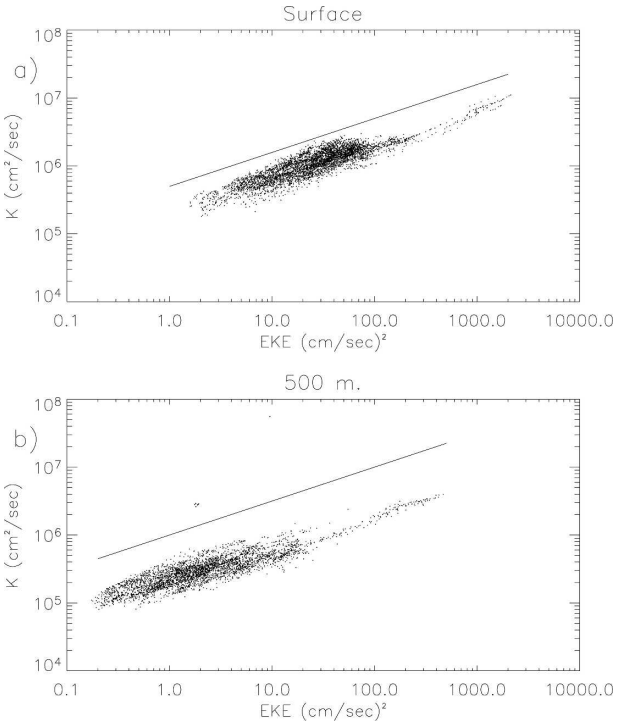

FIG. 17. Bilogarithmic scatterplot of 10-yr-averaged values of eddy diffusivity vs eddy kinetic energy at (a) surface and (b) 500 m of depth. Power law $E^{1/2}$ is superposed. The eddy diffusivity was computed using the parameterization proposed by Babiano et al. (1987) in a Mediterranean OGCM (from Rupolo et al. 2003).

Acknowledgments. Drifters and floats data were obtained from the GDP/SVP and WOCE Data Products Committee. I thank Cara Schock (MEDS) and M. Pazos and R. Lumpkin (NOAA/AOML) for their help in the preprocessing phase of the data. I am also grateful to B. L. Hua, A. Griffa, V. Artale, A. Babiano, and R. Iacono for stimulating discussions. I also acknowledge two anonymous reviewers, since their constructive comments and criticisms helped to improve this work, which was partly supported by the Italian Research Program in Antarctica (CANOPO-PNRA) and by the UE-funded project MFSTEP.

REFERENCES

Babiano, A., C. Basdevant, P. L. Roy, and R. Sadourny, 1987: Single particle dispersion, Lagrangian structure function and Lagrangian energy spectrum in two-dimensional incompressible turbulence. *J. Mar. Res.,* **45,** 107–131.

Bauer, S., M. Swenson, A. Griffa, A. Mariano, and K. Owens, 2002: Eddy mean flow decomposition and eddy-diffusivity estimates in the tropical Pacific Ocean. 2. Results. *J. Geophys. Res.,* **107,** 3154, doi:10.1029/2000JC000613.

Berloff, P., and J. C. McWilliams, 2002: Material transport in oceanic gyres. Part II: Hierarchy of stochastic models. *J. Phys. Oceanogr.,* **32,** 797–830.

——, and ——, 2003: Material transport in oceanic gyres. Part III: Randomized stochastic models. *J. Phys. Oceanogr.,* **33,** 1416–1445.

——, ——, and A. Bracco, 2002: Material transport in oceanic gyres. Part I: Phenomenology. *J. Phys. Oceanogr.,* **32,** 764–796.

Borgas, M., T. Flesch, and B. Sawford, 1997: Turbulent dispersion with broken reflectional symmetry. *J. Fluid Mech.,* **332,** 141–156.

Brink, K., R. Beardsley, P. Niiler, M. Abbott, A. Huyer, R. Samp, T. Stanton, and D. Stuart, 1991: Statistical properties of near-surface flow in the California coastal transition zone. *J. Geophys. Res.,* **96,** 14 693–14 706.

Bryan, K., J. Dukowicz, and R. Smith, 1999: On the mixing coefficient in the parameterization of bolus velocity. *J. Phys. Oceanogr.,* **29,** 2442–2456.

Colin de Verdière, A., 1983: Lagrangian eddy statistics from surface drifters in the eastern North Atlantic. *J. Mar. Res.,* **41,** 375–398.

Davis, R., 1987: Modelling eddy transport of passive tracers. *J. Mar. Res.,* **45,** 635–666.

——, 1991: Observing the general circulation with floats. *Deep-Sea Res.,* **38** (Suppl. 1), 531–571.

Elhmaidi, D., A. Provenzale, and A. Babiano, 1993: Elementary topology of two-dimensional turbulence. *J. Fluid Mech.,* **242,** 655–700.

Figueroa, H., and D. Olson, 1989: Lagrangian statistics in the South Atlantic as derived from SOS and FGGE drifters. *J. Mar. Res.,* **47,** 525–546.

Freeland, H., P. Rhines, and H. T. Rossby, 1975: Statistical observations of the trajectories of neutrally buoyant floats in the North Atlantic. *J. Mar. Res.,* **33,** 383–404.

Griffa, A., 1996: Applications of stochastic particle models to oceanographic problems. *Stochastic Modelling in Physical Oceanography,* R. Adler, P. Müller, and B. Rozovskii, Eds., Birkhäuser, 113–140.

——, K. Owens, L. Piterbarg, and B. Rozovskij, 1995: Estimates of turbulence parameters from Lagrangian data using a stochastic particle model. *J. Mar. Res.,* **53,** 371–401.

Hansen, D. V., and P.-M. Poulain, 1996: Quality control and interpolation of WOCE/TOGA drifter data. *J. Atmos. Oceanic Technol.,* **13,** 900–909.

Hua, B., J. McWilliams, and P. Klein, 1998: Lagrangian accelerations in geostrophic turbulence. *J. Fluid Mech.,* **366,** 151–176.

Kampé de Fériet, J., 1939: Les fonctions aléatoires stationnaires et la théorie statistique de la turbulence homogène. *Ann. Soc. Sci. Bruxelles,* **59,** 145–194.

Krauss, W., and C. W. Böning, 1987: Lagrangian properties of eddy fields in the northern North Atlantic as deduced from satellite-tracked buoys. *J. Mar. Res.,* **45,** 252–291.

Lacasce, J. H., 2000: Floats and f/h. *J. Mar. Res.,* **58,** 61–95.

——, and A. Bower, 2000: Relative dispersion in the subsurface North Atlantic. *J. Mar. Res.,* **58,** 863–894.

Lumpkin, R., and P. Flament, 2000: Lagrangian statistics in the central North Pacific. *J. Mar. Syst.,* **24,** 141–155.

——, and M. Pazos, 2007: Measuring surface currents with Surface Velocity Program drifters: The instrument, its data, and some recent results. *Lagrangian Analysis and Predictability of Coastal and Ocean Dynamics,* A. Griffa et al., Eds., Cambridge University Press, 39–67.

——, A. Treguier, and K. Speer, 2002: Lagrangian eddy scales in the northern Atlantic Ocean. *J. Phys. Oceanogr.,* **32,** 2425–2440.

McWilliams, J., and P. Gent, 1994: The wind-driven ocean circulation with an isopycnal-thickness mixing parameterization. *J. Phys. Oceanogr.,* **24,** 46–65.

Middleton, J. F., 1985: Drifter spectra and diffusivities. *J. Mar. Res.,* **12,** 37–55.

Oh, I., V. Zhurbas, and W. S. Park, 2000: Estimating horizontal in the East Sea (Sea of Japan) and the northwest Pacific from satellite-tracked drifter data. *J. Geophys. Res.,* **105,** 6483–6492.

Pasquero, C., A. Provenzale, and A. Babiano, 2001: Parameterization of dispersion in two dimensional turbulence. *J. Fluid Mech.,* **439,** 279–303.

Poulain, P., and P. Niiler, 1989: Statistical analysis of the surface circulation in the California current system using satellite tracked drifters. *J. Phys. Oceanogr.,* **19,** 1588–1603.

Priestley, M. B., 1981: *Spectral Analysis and Time Series.* Academic Press, 890 pp.

Reynolds, A., 2002: On Lagrangian stochastic modelling of material transport in oceanic gyres. *Physica D,* **172,** 124–138.

Richardson, P., 1993: A census of eddies observed in North Atlantic SOFAR float data. *Progress in Oceanography,* Vol. 41, Elsevier, 127–162.

Riser, S., and H. T. Rossby, 1983: Quasi-Lagrangian structure and variability of the subtropical western North Atlantic circulation. *J. Mar. Res.,* **41,** 127–162.

Rossby, H. T., S. Riser, and A. Mariano, 1983: The western North Atlantic Lagrangian viewpoint. *Eddies in Marine Science,* A. Robinson, Ed., Springer-Verlag, 66–91.

Rupolo, V., B. L. Hua, A. Provenzale, and V. Artale, 1996: Lagrangian spectra at 700 m in the western North Atlantic. *J. Phys. Oceanogr.,* **26,** 1591–1607.

——, A. Babiano, V. Artale, and D. Ludicone, 2003: Sensitivity of the Mediterranean circulation to horizontal space–time-dependent tracer diffusivity field in an OGCM. *Nuovo Cimento,* **26C,** 387–415.

Sawford, B. L., 1991: Reynolds number effects in Lagrangian stochastic models of turbulent dispersion. *Phys. Fluids A,* **3,** 1577–1586.

Shafer Smith, K., and G. K. Vallis, 2001: The scales and the equilibration of midoceanic eddies: Freely evolving flow. *J. Phys. Oceanogr.,* **31,** 554–571.

Stammer, D., 1997: Global characteristics of ocean variability estimated from regional TOPEX/Poseidon altimeter measurements. *J. Phys. Oceanogr.,* **27,** 1743–1769.

——, 1998: On eddy characteristics, eddy transport and mean flow properties. *J. Phys. Oceanogr.,* **28,** 727–739.

Storch, V. H., and F. W. Zwiers, 1999: *Statistical Analysis in Climate Research.* Cambridge University Press, 484 pp.

Taylor, G., 1921: Diffusion by continuous movements. *Proc. London Math. Soc.,* **20,** 196–212.

Treguier, A., I. Held, and V. Larichev, 1997: On the parameterization of quasigeostrophic eddies in primitive equation models. *J. Phys. Oceanogr.,* **27,** 567–580.

Veneziani, M., A. Griffa, A. Reynolds, and A. Mariano, 2004: Oceanic turbulence and stochastic models from subsurface Lagrangian data for the northwest Atlantic Ocean. *J. Phys. Oceanogr.,* **34,** 1884–1906.

Visbeck, M., J. Marshall, and T. Haine, 1997: Specification of eddy transfer coefficient in coarse-resolution ocean circulation model. *J. Phys. Oceanogr.,* **27,** 381–402.

WOCE, 2002: WOCE global data, version 3.0. WOCE International Project Office Rep. 180/02, Southampton, United Kingdom, digital media.

Zambianchi, E., and A. Griffa, 1994: Effects of finite scales of turbulence on dispersion estimates. *J. Mar. Res.,* **52,** 129–148.

Zhang, H., M. D. Prater, and H. T. Rossby, 2001: Isopycnal Lagrangian statistics from the North Atlantic current RAFOS float observations. *J. Geophys. Res.,* **106,** 13 817–13 836.

Zhurbas, V., and I. Oh, 2003: Lateral diffusivity and Lagrangian scales in the Pacific Ocean as derived from drifter data. *J. Geophys. Res.,* **108, 3141,** doi:10.1029/2002JC001596.

——, and ——, 2004: Drifter-derived maps of lateral diffusivity in the Pacific and Atlantic Oceans in relation to surface circulation patterns. *J. Geophys. Res.,* **109, C05015,** doi:10.1029/2003JC002241.